Experimental investigation on micro-ORC system operating with partial evaporation and two–phase expansion

Experimental investigation on micro-ORC system operating with partial evaporation and two-phase expansion

Saverio Ottaviano, Chiara Poletto, Maria Alessandra Ancona, Francesco Melino*

Department of Industrial Engineering, University of Bologna

** Corresponding author: saverio.ottaviano2@unibo.it*

Abstract

This paper presents an experimental analysis conducted on a low-temperature micro-ORC energy system, to assess its performance operating with partial evaporation (PE-ORC). Temperatures of the heat source in the range between 40 °C and 75 °C have been tested, and for each value, the vapour quality at the expander inlet has been varied by regulating the feed-pump rotating speed. The thermodynamic state of the working fluid in two-phase conditions has been estimated by means of a thermal balance at the heat exchangers, using the measured values of temperature, pressure and flow rate.

Detailed experimental results are provided, with special focus on the performance of evaporator, expander and feed-pump, highlighting the difference in their behaviour compared with the regular operation with dry expansion of the same micro-ORC system. Relevant improvements have been observed in the evaporator effectiveness, mainly due to the reduction of the pinch point temperature difference. Also, the volumetric and total efficiencies of the feed-pump are improved substantially. On the other hand, the net power output and the expander efficiency resulted penalized by the operation with partial evaporation. The maximum power output obtained was close to 1.2 kW, with heat source temperature equal to 75 °C and fluid quality close to 1. The power output is reduced, at constant temperature, by decreasing the vapour quality at the expander inlet.

The results suggest that operating a small-scale ORC system with partial evaporation may lead to some improvements to the performance of the cycle, especially regarding the evaporator performance. Moreover, with values of fluid quality at the expander inlet between 0.8 and 1, the penalization on the expander performance, compared to the dry expansion mode, is limited. However, a proper redesign of the power plant for the specific purpose is required in order to make partial evaporation an effective solution. Specifically, the expander and pump geometry and control require to be optimized for the particular working conditions, the recuperator must be removed, and the evaporator should be designed for the optimal exploitation of the heat source.

Nomenclature

Symbols and acronyms

A	Surface area [m^2]
BWR	Back Work Ratio [%]
c	Specific heat [kJ/(kg K)]
DE	Dry expansion
E	Error
f	Frequency [Hz]
FF	Filling Factor [-]
FS	Full Scale
h	Specific enthalpy [kJ/kg]
I/O	Input/output
$\dot{m}$	Mass flow rate [kg/s]
N	Rotational speed [rpm]
ORC	Organic Rankine Cycle
p	Pressure [bar]
PE	Partial evaporation
$\dot{Q}$	Thermal power [kW]
RV	Reading value
T	Temperature [°C]
U	Uncertainty / Heat transfer coefficient [kW/(m^2 K)]
$\dot{V}$	Volumetric flow rate [l/s]
$\dot{W}$	Power [W]
x	Vapor quality in the two-phase mixture [-]

Greek letters

η	Efficiency [-]
ε	Heat transfer effectiveness [-]
ρ	Density [kg/m^3]
τ	Temperature difference [K]

Subscripts

CW	Cold water
cond	Condensation/condenser
el	Electric
eco	Economizer
eva	Evaporator
exp	Expander
HW	Hot water
in	Inlet
is	Isentropic
L	Liquid phase (saturation)
out	Outlet
pump	Pump
rec	Recuperator
sh	Superheating
th	Thermodynamic (referred to power)
V	Vapor phase (saturation)
vap	Vaporization / vaporizer

1. Introduction

Supporting the green transition also involves reducing the waste of thermal energy that could be available for conversion into electricity. It is well known that a huge amount of thermal energy at low temperature is discharged to the ambient as waste heat. On a global scale, it was estimated that 12.6% of the primary energy supplied to the industrial sector is released at temperatures lower than 100 °C [1], [2]. Moreover, in some applications, this thermal power must be dissipated by being transferred to a cooling system, which generally consumes electricity to operate. Recovering such heat to produce electrical power may represent a valuable solution for increasing the global effectiveness of primary energy conversion processes.
The organic Rankine cycle is considered the most suitable technology for the conversion of low-temperature heat sources into electricity. However, at present, ORCs are mostly employed within the small-to-medium size field, while the micro-size (power lower than 50 kW) is not commonly

employed, and research is still ongoing to improve the performance and optimize this class of energy systems. The main advances that are currently studied regard: the optimization of the expander, which usually in the micro-size is a volumetric machine (mostly piston, vane, screw or scroll, generally derived from HVAC compressor) [3]; the selection of the right working fluid for each specific application; the reduction of the feed-pump consumption, which represents a considerable contribution to the conversion losses; the development of control strategies to increase the performance in case of dynamic conditions of the heat source and in off-design operation; the analysis of non-conventional cycles able to enhance the conversion efficiency. Concerning this last point, the ORC with partial evaporation and two-phase expansion is gaining attention due to some distinctive characteristics that make it profitable for the exploitation of low-grade heat sources. If the expansion occurs entirely in wet conditions, generally two configurations are possible (see Figure 1):

a) the trilateral flash cycle (TFC), in which the fluid enters the expander in the state of saturated liquid, or with vapour quality lower than 0.1 (Figure 1*a*). In this case, the evaporator has the task of heating up the fluid to its vaporization temperature. In other words, the evaporator assumes the function of an economizer, while the actual vaporization process does not start inside the heat exchanger. The only vapour that expands in the expander is that generated by the pressure drop (flash vapour);

b) the partially evaporated organic Rankine cycle (PE-ORC), in which the vaporization of the working fluid is interrupted at a certain value of the vapour quality (Figure 1*b*). Compared to the previous case, a larger amount of fluid vapour is expanded inside the expander, and in the evaporator both sensible and latent heat is transferred. This solution may be adopted to reduce some of the drawbacks that characterize the TFC.

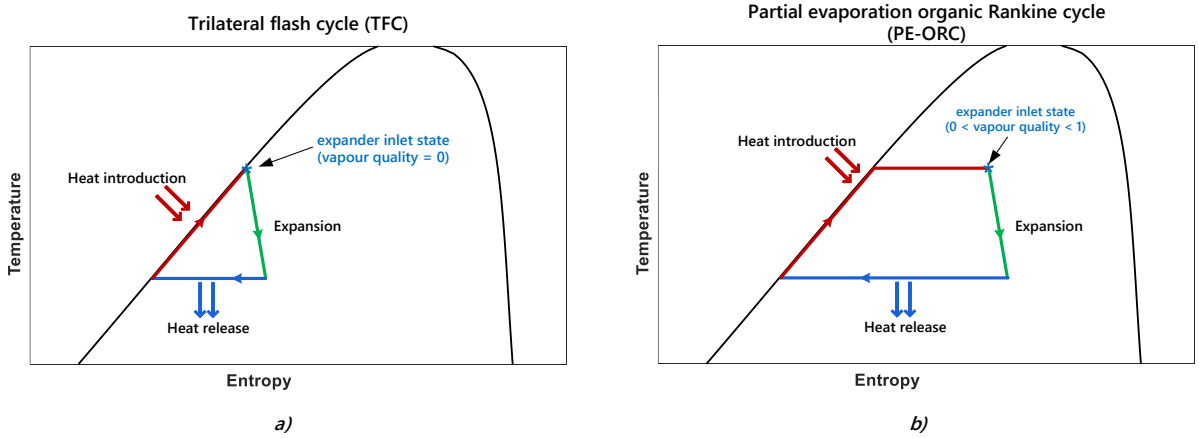

Figure 1 - generic representation of trilateral flash cycle (TFC) (a), and partial evaporation organic Rankine cycle (PE-ORC) (b).

The interest in studying ORC systems with trilateral cycle or partial evaporation regards the possibility to achieve higher conversion efficiency from heat sources with a finite capacity [4],

[5]. Indeed, eliminating or reducing the isothermal heat of vaporization allows for an improvement of the temperature match between the heat source and the working fluid, resulting in higher usage of the energy available from the heat source. This condition reduces heat transfer losses and increases the heat exchanger effectiveness. It was observed that the largest convenience is achieved with low-temperature heat sources [6].

On the contrary, the performance of the expander in wet conditions may be lower than in the case of dry expansion, resulting in lower power output at a given mass flow rate of the working fluid. Moreover, the expansion occurring in the two-phase condition, in general, may lead to erosion of the expander materials that reduces the machine lifetime [7]. Regarding this aspect, it is well known that, with respect to turbines, volumetric expanders can withstand better the expansion occurring, partially or completely, in the two-phase condition [8].

Several articles deal with theoretical assessment of TFC and PE-ORC, with the purpose of optimization, design, or techno-economic analysis. For example, Lai et al. [9] presented a thermodynamic model to compare the optimal performance of ORC and TFC, with different working fluids and a heat source temperatures of 80 °C, investigating the effect of the pinch point temperature. They obtained a higher net power output with the TFC of approximately 30% with respect to the ORC. McGinty et al. [10] performed a techno-economic survey of a 2-MW TFC varying the working fluid and the heat source temperature. Based on simulation results, they also developed a scaled pilot test bench with a twin-screw expander and R245fa as working fluid, which was able to produce a maximum power output of 6.2 kW, with a cycle efficiency around 4%. A modelling study on a TFC has been presented by Skiadopoulos et al. in [11]. In their model, a semi-empirical approach was used for simulating the two-phase expansion in a twin-screw expander working with R113. Wang et al. [12] proposed a thermodynamic model of a two-phase reciprocating expander using water, with a flash chamber for TFC applications. They adopted an intake ratio to analyse the cylinder intake process of saturated liquid and the corresponding losses. Results highlighted the linear increase in the intake losses with the increment of the intake ratio, and a corresponding decrease in the expander isentropic efficiency. White [13] investigated a two-phase ORC system operating with wet-to-dry expansion using a radial-inflow turbine. They conducted an optimization procedure of the cycle and of the turbine performance, changing the working fluid amongst hydrocarbons and siloxanes with dry characteristic. The adoption of a radial-inflow turbine assures higher expander isentropic efficiencies, while in their calculation the two-phase expansion improves the power output from waste-heat recovery systems by up to 30% [13].

The lack of experimental data on two-phase expansion represents an important limit to the research in this field. Indeed, not many experimental studies have been published during the last decades on Rankine cycles with wet expansion, and the majority are referred to screw expanders. For example, Steidel et al. [14] tested a twin-screw expander with geothermal water, varying the vapour quality at the expander inlet between 8% and 27%, and obtaining a maximum efficiency of 53%. Smith et al. [15] conducted an experimental analysis on a twin-screw machine using R113 as working fluid; they concluded that isentropic efficiency up to 70% may be obtained for sizes of the system below 25 kW, and even higher than 80% for large scale power plant operating with two-phase expansion. The analysis of Ohman and Lundqvist [16] was conducted on a Lysholm turbine operating with R134a, with the aim of comparing the performance of the machine in case of superheated, saturated and two-phase conditions of the working fluid at the expander inlet. They obtained an expander efficiency close to 80% with a vapour quality of 0.7. Iqbal et al. made an experimental investigation on a TFC-based system working with iso-

pentane, with the expansion performed thanks to a converging-diverging nozzle and a Pelton turbine. Their test rig was essentially demonstrative, as the power output was only of few watts; nevertheless, they obtained thermal efficiency up to 14% with heat source temperature between 64°C and 75°C [17]. Dawo et al. performed an experimental comparison between the ORC and the PE-ORC operating modes, using the same test rig and R1233zd(E) as working fluid. They varied the heat source temperature between 110 °C and 140 °C and the vapour quality in the range 0.20-0.40, finding that the ORC with a fixed superheating degree of 10 K presents higher thermal efficiency, while the PE-ORC is characterized by better heat transfer efficiency, especially at lower values of heat source temperature [18].
To the Authors' knowledge, very few studies deal with reciprocating piston expanders working with wet expansion. In the paper presented by Kanno and Shikazono, an experimental analysis is conducted on the two-phase adiabatic expansion in a single cylinder, achieving isentropic efficiency of 86% and 82% with water and ethanol as working fluids, respectively [19]. Another experiment was performed by Löffler on a flash process in a cyclone, which separates the steam that then is expanded in a cylinder of a piston engine [20].

1.1. Aim of the study

This paper presents an experimental analysis on a micro-ORC system operated with partial evaporation and two-phase expansion. The analysis is conducted in steady-state conditions, at different values of the hot water temperature. For each condition of the heat source, the feed-pump speed is regulated to increase the mass flow rate of the working fluid, which influences the value of the vapour quality at the expander inlet. The results of the campaign are compared with those obtained with the same micro-ORC system in its regular operation, i.e. in dry expansion conditions (these results have been presented in [21], [22]).
The main novelties of this study can be summarized as follows:

- the experimental investigation of a residential-scale ORC system working in PE mode is reported in detail, with focus on both the overall cycle and the main components (especially expander, pump, evaporator); other studies that can be found in the literature are focused of the analysis of the expansion process ([16], [19]). The comprehensive set of experimental data is provided in the Appendix, and it may be used by researchers for model validation or for design purposes.
- Very low-quality heat is considered, as the system is tested with heat source temperature in the range 40-75 °C; in previous studies the minimum tested temperatures are above 80 °C ([18], [19]).
- The two-phase expansion in a kW-scale piston expander is demonstrated experimentally, and the expander performance investigated; in most of the experimental studies, different types of expander are employed, mostly screw expanders ([14], [15], [16], [18]).

2. Description of the micro-ORC test bench

The micro-ORC energy system installed in the micro-generation laboratory of the University of Bologna is a kW-size test rig, conceived to exploit low-temperature heat sources in residential applications. Figure 2 shows the test rig layout, which is composed of three circuits: the internal ORC circuit and two external circuits of hot and cold water, namely the heat source and the cooling system. A photo of the installation is presented in Figure 3.

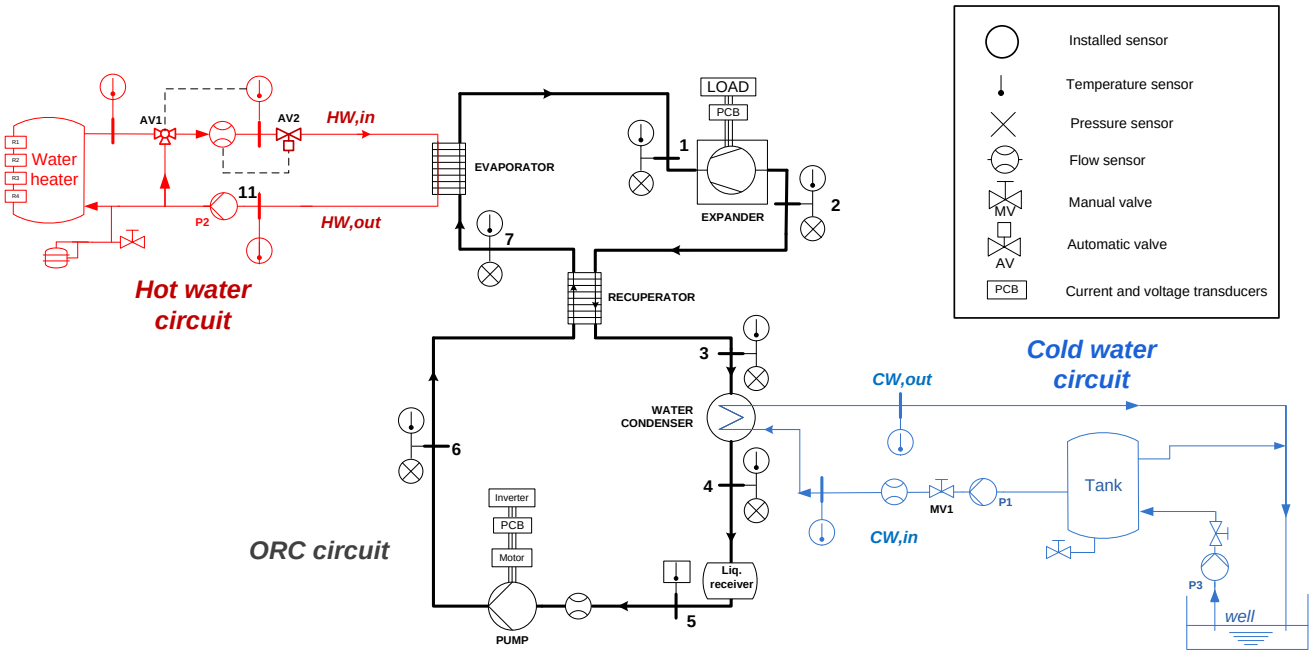

Figure 2 – Layout of the micro-ORC test bench

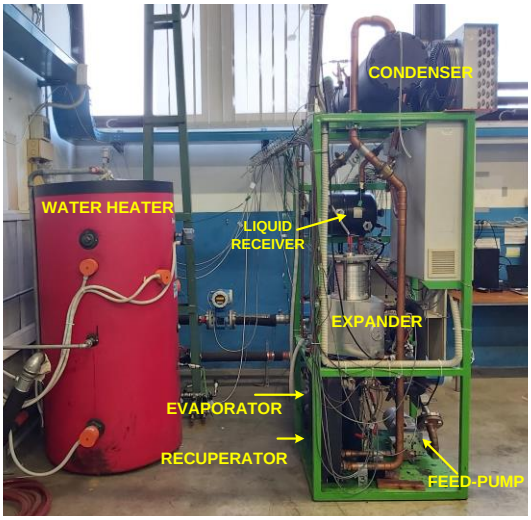

Figure 3 – photo of the test bench.

The ORC circuit, based on a recuperative configuration, operates with HFC-134a (R134a) as working fluid with a total charge of 22 kg. The main components of the ORC circuit are a reciprocating pistons expander, an external gear pump, two brazed plate heat exchangers (the evaporator and the recuperator), a shell and tube condenser and a liquid receiver. Table 1 collects the specifics of the main components of the ORC circuit.

Table 1 – main specifics of the micro-ORC components

COMPONENT	MODEL	FEATURES
EVAPORATOR	ONDA S202	Plate heat exchanger with 64 plates
RECUPERATOR	ONDA S202	Plate heat exchanger with 19 plates
CONDENSER	ONDA CT292-1100	Shell-and-tube heat exchanger with 4 passages
EXPANDER	Radial piston prototype (STARENGINE) [24]	Three radial cylinders at 120°, displacement = 230 cm^3, direct coupling with generator
PUMP	External gear prototype (STARENGINE)	Displacement = 50 cm^3, driven by three-phase 1.5 kW asynchronous motor with inverter. Variable speed between 90 rpm and 300 rpm
GENERATOR	Magnetic NGB 145 M-SA	Three-phase permanent magnet synchronous generator, 380 V, 5.2 A, 8 poles
LOAD	Pure resistive	Five parallel loads, each made of three light bulbs, connected in *delta* with the generator

The heat transfer surfaces of the three heat exchangers have been estimated using available geometrical parameters, and resulted equal to 10.21 m^2 for the evaporator, 2.80 m^2 for the recuperator, and 2.85 m^2 for the condenser. The hot source is composed of an electric water heater with nominal thermal power of 42 kW, consisting of a 500-litres tank provided with five heating elements, which can be activated separately to regulate the thermal input to the ORC evaporator. The pressure inside the hot water circuit is maintained above the ambient pressure (between 1 and 2 bar), in order to avoid local vaporization phenomena at high temperatures, which may cause the cavitation of the centrifugal pump P2. The water temperature at the evaporator inlet can be regulated using the automatic three-way valve (AV1) placed at the heater outlet, which mixes the hot water with colder water coming from the evaporator. The water flow rate is adjusted by acting on the motorized ball valve (AV2). The electrical load consists of five pure resistive loads, connected in parallel between them and in *delta* with the generator output three-phase line. Each load is composed by three light bulbs with nominal power of 200 W each, and is provided with a separate switch, so the power load is adjustable between 600 W and 3000 W. With this load configuration, the expander rotational speed is the result of the equilibrium between the driving and the load torque.

The specifications of the measurement devices are collected in Table 2. In short, the list of measured variables includes temperatures, pressures and mass flow rate in ORC circuit, temperatures and volume flow rates in hot and cold water circuits, electric current and voltage of expander and feed-pump for power and frequency assessment. The number and positions of the sensors are detailed in Figure 2 and in Table 2. All pressure transducers and thermocouples are calibrated periodically at the laboratory, together with the complete measurement chain (cables and acquisition devices), in order to decrease the uncertainty related to the performance assessment. The acquisition system is developed on a National Instruments CompacRIO in

LabVIEW environment. The properties of the organic fluid are computed thanks to the open-source library CoolProp [25], which is integrated into the acquisition software.

Table 2 – sensors specifics.

PHYSICAL QUANTITY	LAYOUT POINT (FIGURE 2)	SENSOR	CALIBRATION RANGE	COTS ACCURACY*	OUTPUT SIGNAL AND MODULE
ORC TEMPERATURES	1, 2, 3, 4, 6, 7	T-type thermocouple, 1 mm probe	0–90 °C	±0.5 °C	±80 mV - NI9213 (Thermocouple input)
HOT WATER TEMPERATURES	HW_{in}, HW_{out}, HW_{boil}	K-type thermocouple, 1 mm probe	0–90 °C	±0.5 °C	
COLD WATER TEMPERATURES	CW_{in}, CW_{out}				
ORC PRESSURES	1, 6, 7	Pressure transducer, Honeywell FP2000	0–30 bar	±0.25% FS	0–5 V - NI9201
	2, 3, 4, 5		0–10 bar		
ORC MASS FLOW RATE	5	Coriolis mass flow meter, E+H Promass	0.05–1.00 kg/s	±0.3% RV	4–20 mA - NI9203
ORC DENSITY			10–1300 kg/m3	±0.1 kg/m3	
HOT WATER FLOW RATE	HW_{in},	Magnetic flow meter, E+H Promag	0–6.4 l/s	±0.5% RV	
COLD WATER FLOW RATE	CW_{in}		0–9.8 l/s		
ELECTRIC VOLTAGE AND CURRENT	Expander generator and pump motor supply lines	PCB-mounted Hall effect voltage and current transducers	0–400 V	±0.1% RV	0–4 V - NI9215
			0–5A	±0.2% RV	

*Component Off-the-Shelf (COTS) accuracy: it refers to the instrument accuracy, as indicated on the datasheet, before individual calibration or calibration of the measurement chain.

3. Tests methodology

The experimental analysis is conducted imposing different levels of hot water temperature at the evaporator inlet ($T_{HW,in}$). Keeping constant $T_{HW,in}$ and the hot water flow rate ($\dot{m}_{HW}$), the flow rate of the working fluid ($\dot{m}_{wf}$) is changed acting on the feed-pump frequency (f_{pump}), setting the pump rotational speed. The transition from DE to PE operation is represented qualitatively in the temperature-entropy diagrams of Figure 4, in which the vaporization process is compared in three cases, characterized by constant heat source temperature (yellow line). Figure 4*a* represents a dry expansion case characterized by low mass flow rate, low evaporation pressure and high superheating degree at the expander inlet (point 1 in Figure 2). Increasing the value of $\dot{m}_{wf}$, the evaporation pressure also increases while the superheating degree is reduced, as shown in Figure 4*b*, where the superheating degree is assumed to be the minimum that ensures the dry expansion. A further increment of the mass flow rate leads to the condition represented in Figure 4*c* (PE mode), in which the vaporization process is interrupted and the working fluid at the expander inlet is in the two-phase conditions. Once the system operates in the PE mode, continuing increasing the mass flow rate will reduce the vapour quality of the working fluid at the expander inlet, at constant evaporation pressure.

The value of vaporization temperature (and pressure) in the PE case is affected, besides the hot water temperature and the working fluid flow rate, by the hot water flow rate, $\dot{m}_{HW}$. Considering, in a first approximation, a constant temperature difference at the evaporator pinch

point, the increment of $\dot{m}_{HW}$ leads to a reduction of the slope of the water curve in the heat transfer diagram of the evaporator, and therefore to an increment of the evaporation temperature and pressure. However, within the operating conditions tested in this campaign, the effect of the hot water flow rate on the cycle pressure is limited, compared to the effect of the water temperature.

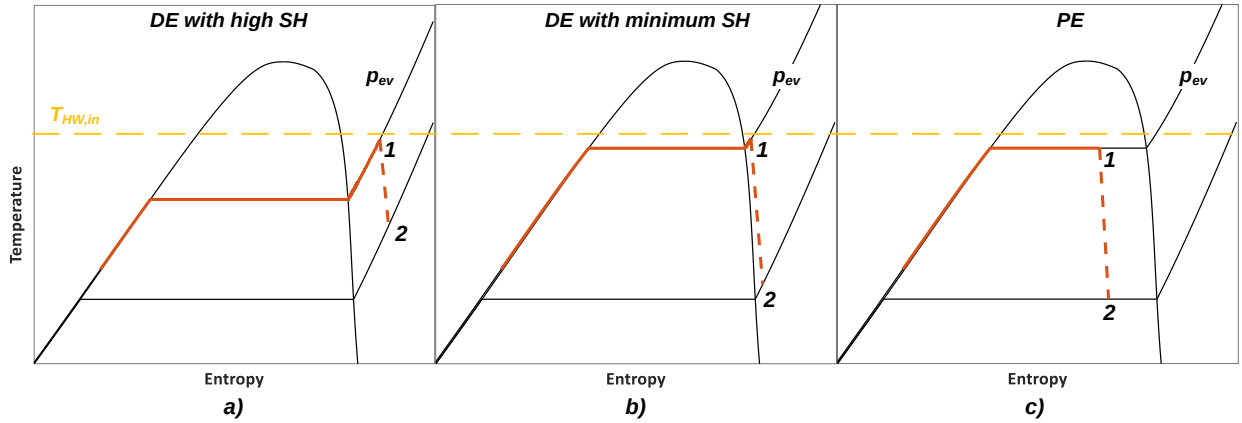

Figure 4 – Comparison of three vaporization processes, at constant heat source temperature: dry expansion with high superheating degree (a), dry expansion with minimum superheating degree (b) and partial evaporation (c).

In the test bench under investigation, the minimum achievable value of the quality depends on three key limiting factors: i) the maximum pump rotating frequency, which affects the maximum flow rate of the working fluid, ii) the heat source temperature, which constrains the evaporation temperature and pressure, and iii) the maximum pressure inside the circuit. At $T_{HW,in}$ higher than 80 °C, for example, the evaporating pressure exceeds the value of 26 bar, which is the set limit of the safety valve for preserving the test bench components. Moreover, the maximum frequency of the feed-pump limits the possibility to achieve vapour quality close to zero (saturated liquid) at high heat source temperature.

3.1. Boundary conditions

The set points of the experimental tests are identified by the level of the heat source temperature ($T_{HW,in}$), which is varied from 40 °C to 75 °C, and by the frequency of the feed-pump, increased within the range 15 Hz - 60 Hz, corresponding to a rotational speed of the pump shaft between 75 rpm and 300 rpm. The set of boundary conditions is displayed in Figure 5 in terms of heat source temperature and pump frequency. The cross markers indicate the operating points in dry expansion (DE) mode. The DE points are all characterized by a value of superheating degree at the expander inlet between 3 K and 7 K, corresponding to the minimum range for assuring the expansion to occur in dry conditions.
Figure 6 reports for the Reader's convenience the curve of the saturation pressure as function of the temperature, for the fluid HFC-134a. In the range of heat source temperature tested in this campaign, the expected values of the evaporation pressure are between 9 bar and 22 bar, as highlighted in Figure 6, corresponding – under the assumption of cooling water at ambient temperature between 10 °C and 20 °C – to a potential pressure difference (Δp_{exp}) in the range 3-16 bar.

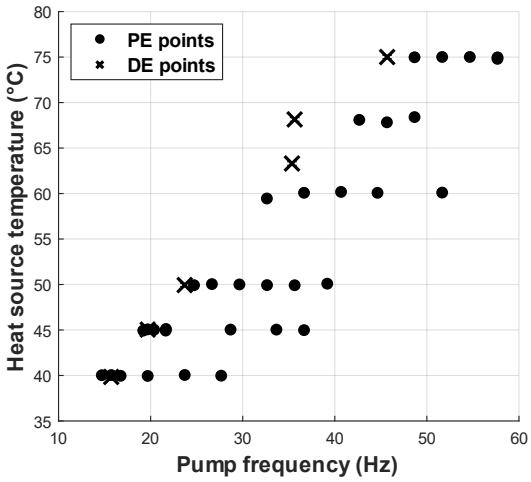

Figure 5 – experimental set points.

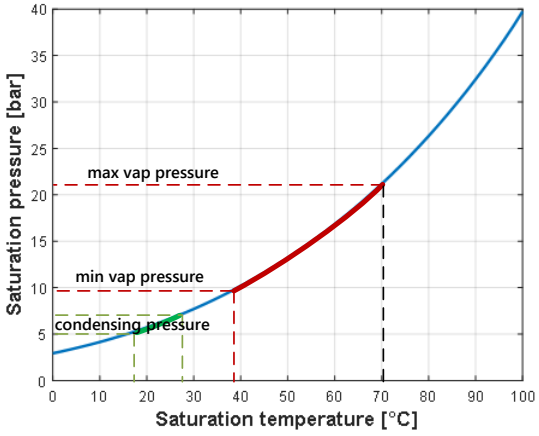

Figure 6 – Saturation pressure as function of the evaporation temperature; the operating ranges involved in this study are highlighted.

3.2. Assessment of the thermodynamic properties in PE conditions

The thermodynamic state of the working fluid in single phase conditions (subcooled liquid or superheated vapour) is determined directly using the CoolProp function [25], with temperature and pressure values as inputs. This is expressed by Equation (1), where the term *CPfun* indicates the CoolProp function, and the subscript *i* recall the number of the ORC section, according to the layout in Figure 2.

$$h_i = CPfun(p_i, T_i) \qquad i = 4, 5, 6, 7 \tag{1}$$

When the ORC system operates with partial evaporation, complete information about the thermodynamic state of the working fluid at point 1, 2 and 3 (corresponding to expander inlet and outlet, and recuperator outlet, respectively) are not available directly from measurements. Indeed, if the fluid is in two-phase condition, the knowledge of temperature and pressure is not sufficient to determine the corresponding fluid enthalpy or the vapour quality.
Therefore, to estimate the complete thermodynamic states of the system working in PE mode, a thermal balance has been performed on the heat exchangers, to calculate the enthalpy values in the two-phase region. In particular, the specific enthalpy of the working fluid at the evaporator outlet (or at the expander inlet, h_1) is calculated, according to Equation (2), applying the thermal balance at the evaporator. The enthalpy of the fluid entering the evaporator (h_7) is obtained regularly as CoolProp function of measured temperature and pressure (T_7 and p_7, respectively), since the fluid at the evaporator inlet is in the subcooled phase.

$$h_1 = h_7 + \frac{\dot{V}_{HW} \cdot \rho_{HW}}{\dot{m}_{wf}} \cdot c_{HW} \cdot \left(T_{HW,in} - T_{HW,out}\right) \tag{2}$$

In Eq. (2), the symbols $\dot{V}_{HW}$, ρ_{HW} and c_{HW} represent, respectively, the volume flow rate, the density and the specific heat of the water. The rigorous values of density and specific heat are computed via CoolProp as functions of measured temperature and pressure of the hot water.
In similar way, the fluid enthalpy at the condenser inlet (h_3) is calculated by means of the heat balance in the condenser, according to Equation (3). In this case, the enthalpy of the subcooled liquid at the condenser outlet (h_4) is determined by means of the CoolProp library as function of temperature and pressure. Finally, the enthalpy value at the expander outlet (h_2) is obtained from Equation (4), which represents the thermal balance in the recuperator, assuming constant mass flow rate of the working fluid in the whole ORC circuit.

$$h_3 = h_4 + \frac{\dot{V}_{CW} \cdot \rho_{CW}}{\dot{m}_{wf}} \cdot c_{CW} \cdot \left(T_{CW,out} - T_{CW,in}\right) \quad (3)$$

$$h_2 = h_3 + (h_7 - h_6) \quad (4)$$

Additional terms related to heat losses are not included in the balance equations (2)-(4). This assumption relies on the fact that the evaporator and the recuperator are thermally insulated, while the condenser works at temperature very close to the ambient temperature; thus, the thermal losses in the three heat exchangers can be considered negligible.
Once the enthalpy has been computed in all the sections of the circuit, the thermodynamic cycle of the PE-ORC is fully determined. The values of the vapour quality in the two-phase points (1, 2 and 3) are obtained using pressure and enthalpy as inputs to the CoolProp library, as indicated in Equation (5).

$$x_i = CPfun(p_i, h_i) \qquad i = 1,2,3 \quad (5)$$

3.3. Performance indexes

Once all the thermodynamic states have been determined, it is possible to calculate the performance of the system. The ORC global efficiency (η_{ORC}) is calculated according to Equation (6), as the ratio between the net electric power ($\dot{W}_{net}$) and the thermal power transferred in the evaporator ($\dot{Q}_{eva}$). $\dot{W}_{exp,el}$ and $\dot{W}_{pump,el}$ are the measured values of the electric power of the expander and of the pump, respectively. The second law efficiency, η_{II}, is calculated, according to Equation (7), as the ratio between the global efficiency and the equivalent Carnot efficiency (η_{Carnot}), evaluated at the same values of hot source and cold sink temperatures. The ratio between the pump consumed power and the expander power output, commonly referred as back work ratio (BWR, Equation (8)), is a crucial parameter especially in small-scale ORCs operating with low-critical temperature fluids; in such systems, the impact of the pump consumption on the net power output is significant (greater than 10%), even in well-designed plants [7].

$$\eta_{ORC} = \frac{\dot{W}_{net}}{\dot{Q}_{eva}} = \frac{\dot{W}_{exp,el} - \dot{W}_{pump,el}}{\dot{m}_{wf} \cdot (h_1 - h_7)} \quad (6)$$

$$\eta_{II} = \frac{\eta_{ORC}}{\eta_{Carnot}} = \frac{\dot{W}_{exp,el} - \dot{W}_{pump,el}}{\dot{Q}_{eva}} \cdot \frac{1}{1 - {T_{CW,in}}/{T_{HW,in}}} \quad (7)$$

$$BWR = \frac{\dot{W}_{pump,el}}{\dot{W}_{exp,el}} \quad (8)$$

The expander efficiency (η_{exp}) is calculated according to Equation (9), where the term $h_{2,is}$ is the value of the specific enthalpy at the expander outlet in the ideal (isentropic) expansion. The expander filling factor (FF) has the expression reported in Equation (10), where ρ_1 corresponds to the density at the expander inlet, N_{exp} is the rotating speed in rpm, and V_{exp} is the expander total displacement. The total efficiency of the feed-pump (η_{pump}) is computed according to Equation (11), as the ratio between the ideal hydraulic power and the electric power consumed by the pump. The symbol ρ_5 refers to the density at the pump inlet, which is measured directly by the Coriolis flow meter. Finally, Equation (12) is used to compute the volumetric efficiency of the pump ($\eta_{pump,vol}$), with N_{pump} and V_{pump} corresponding, respectively, to the pump rotational speed in rpm and to the pump displacement.

$$\eta_{exp} = \frac{\dot{W}_{exp,el}}{\dot{m}_{wf} \cdot (h_1 - h_{2,is})} \quad (9)$$

$$FF = \frac{\dot{m}_{wf}}{\rho_1 \cdot N_{exp}/60 \cdot V_{exp}} \quad (10)$$

$$\eta_{pump} = \frac{\dot{m}_{wf} \cdot (p_6 - p_4)}{\rho_5 \cdot \dot{W}_{pump,el}} \quad (11)$$

$$\eta_{pump,vol} = \frac{\dot{m}_{wf}}{\rho_5 \cdot N_{pump}/60 \cdot V_{pump}} \quad (12)$$

3.1 Measurements and calculation uncertainty

The assessment of the thermodynamic state in the two-phase region is based on thermal balances and CoolProp functions applied to multiple variables, each adding a contribution to the total uncertainty of the calculated state property. The uncertainty calculation of the ORC performance parameters, which has been described in [23], is based on the procedure reported in the standard

ISO/IEC Guide 98 and EA-4/02M. The propagation of the uncertainty is evaluated by means of the classic procedure based on the propagation rule: this rule allows to calculate the uncertainty of a variable by considering the uncertainties of all the variables from which it depends. For instance, if y is a variable computed as a function of x and z, the uncertainty of y, δy, is evaluated through Equation (13).

$$\delta y = \sqrt{\left(\frac{\partial y}{\partial x}\right)^2 \delta x^2 + \left(\frac{\partial y}{\partial z}\right)^2 \delta z^2} \tag{13}$$

where δx and δz are the uncertainties of x and z, while $\frac{\partial y}{\partial x}$ and $\frac{\partial y}{\partial z}$ are the partial derivatives of y with reference to respectively x and z.

Amongst the three standards for the computation of the uncertainty contributions presented in [23], the present case belongs to the Primary Laboratory Standard, in which the measurement uncertainty is represented by the reference uncertainty of the certified laboratory. This is the case of temperature, pressure and electric power sensors, which are calibrated periodically at our laboratory in their operating ranges with certified instrument. The uncertainty contributions of the flow rate measurements, instead, are based on the accuracy provided by the manufacturer (off-the-shelf accuracy). In the figures presented in the next section, the data are plotted with their corresponding error bands obtained applying the above-mentioned procedure.

4. Experimental results and discussion

The results reported in this section are related to experimental tests conducted in steady-state conditions, and are presented as average values calculated in time intervals in which the key variables showed constant trends. The criterion for the steady-state detection is derived from that applied in [26], in which a variable is considered steady if its variation around the average value is within ±2% for a time interval of 600 seconds. However, by conducting experiments at constant heat source temperature, it was observed that the operation with partial evaporation involves very few and limited transient conditions. Indeed, the variation of the mass flow rate in saturation conditions does not produce a significant change in the evaporation and condensation pressures and temperatures, while the main effect is the variation of the vapour quality of the two-phase mixture. For this reason, the minimum time interval for the steady-state operation has been reduced to 400 s, as such value is recognized sufficient for the full stabilization of the key acquired variables after a perturbation.

It is interesting to visualize the comparison of the experimental results obtained in partial evaporation (PE) mode with those acquired with superheating conditions at the expander inlet (or in dry expansion mode – DE), at the same temperatures of the heat source. In order to simplify the comparison to the Reader, in the following figures the data acquired in DE mode are displayed with cross markers.

Considering that the test rig is not optimized for partial evaporation, the relevance of the results should be examined mostly from a qualitative point of view, in terms of trends and dependencies of the performance variables, and focusing on the comparison with the dry expansion operation.

4.1. Operating conditions and overall performance

In PE conditions, the trend of the mass flow rate of the working fluid ($\dot{m}_{wf}$), as function of the pump frequency (f_{pump}), is similar to that of the DE operation, but a slight increment of $\dot{m}_{wf}$ is registered at constant frequency in the PE mode (see Figure 7). The value of the flow rate increases with the increment of the pump frequency, varying from a minimum close to 40 g/s at 15 Hz, to a maximum of almost 250 g/s at 58 Hz. A secondary effect on the mass flow rate is given by the level of the heat source temperature, whose increment is associated to a slight reduction of the flow rate at the same pump frequency.

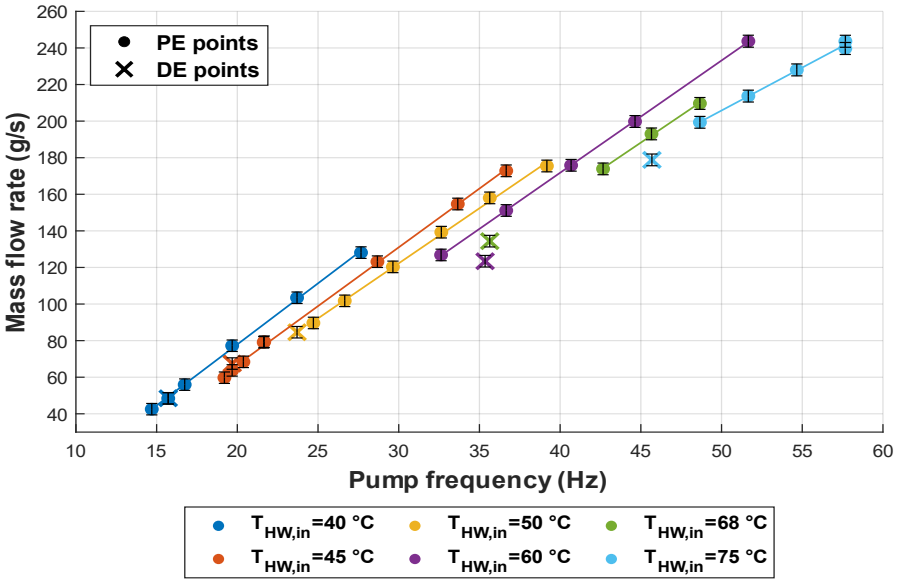

Figure 7 – working fluid mass flow rate versus pump frequency, varying the heat source temperatures

Figure 8 shows the trend of the evaporation pressure (p_1) versus the mass flow rate, at different values of the hot water temperature. It is observed that the value of p_1 depends mainly on the heat source temperature, varying between 9 bar and 21 bar with $T_{HW,in}$ that increases from 40 °C to 75 °C. This behaviour is in contrast with the operation in dry expansion mode, in which the increment of the flow rate leads in general to an increment of the evaporation pressure. Indeed, one main effect of the partial evaporation is that the evaporating pressure remains almost constant varying the mass flow rate of the working fluid, at constant $T_{HW,in}$. Furthermore, it has been observed experimentally that the condensation pressure (p_2) does not present significant variation at the different conditions of pump rotating frequency; thus, also the pressure difference across the expander is only scarcely affected by the change of the mass flow rate, while a more relevant effect is given by the heat source temperature.
As soon as the saturation condition is achieved, the increment of the flow rate causes the reduction of the vapour quality at the expander inlet (x_1), as shown in Figure 9, which reports the quality as a function of mass flow rate and hot water temperature. Different trends are related to different values of $T_{HW,in}$: at constant mass flow rate, a lower value of x_1 can be achieved with lower temperatures. At constant hot water temperature ($T_{HW,in}$), the vapour quality decreases as

the working fluid mass flow rate ($\dot{m}_{wf}$) is increased. With the maximum tested value of heat source temperature, equal to 75 °C, the saturation condition ($x_1 \cong 1$) is achieved with a flow rate around 200 g/s, while the minimum quality is slightly above 0.7, obtained with $\dot{m}_{wf}$ close to 250 g/s (corresponding to a pump frequency of 58 Hz, close to the maximum settable value of 60 Hz). The minimum value of vapour quality, close to 0.20, is obtained with low hot water temperature ($T_{HW,in} = 40°C - 45\ °C$), and with mass flow in the range 130-170 g/s. The higher is the hot water temperature, the higher is the minimum value of mass flow rate in order to operate with partial evaporation ($x_1 < 1$). It is observed that with heat source temperatures equal to 40 °C and 45 °C, the minimum frequency of the feed-pump (16-18 Hz) causes already the two-phase condition at the expander inlet, with vapour quality between 0.95 and 1.0. Therefore, the partial evaporation might be, for the ORC system under investigation, the only operating option if the evaporator is supplied with a $T_{HW,in}$ lower than 45 °C.

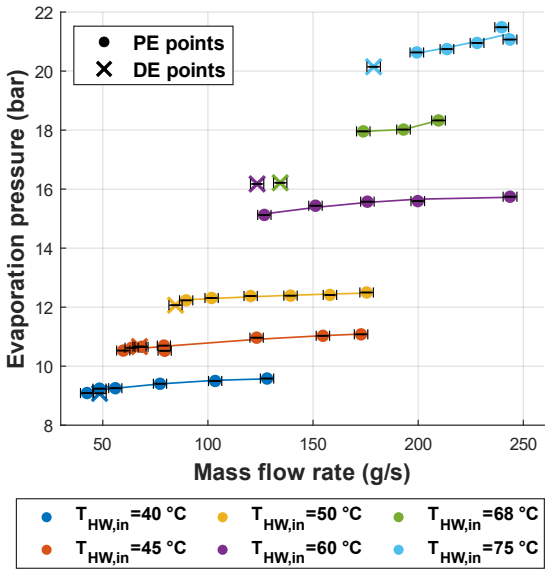

Figure 8 – evaporation pressure (p_1) versus working fluid mass flow rate ($\dot{m}_{wf}$), at different heat source temperatures ($T_{HW,in}$).

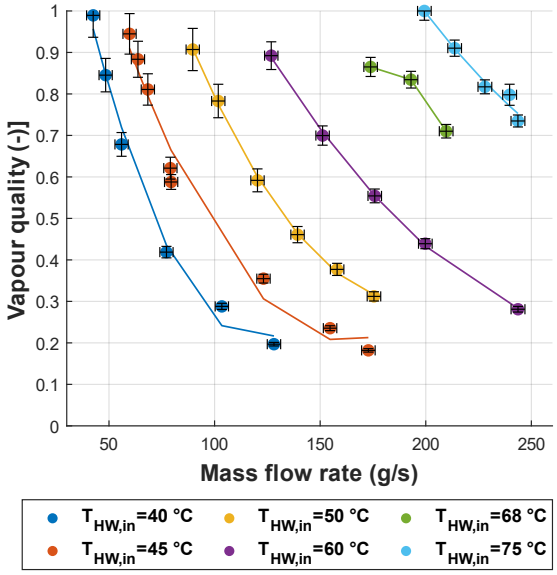

Figure 9 – vapour quality at the expander inlet (x_1) versus working fluid mass flow rate ($\dot{m}_{wf}$), at different heat source temperatures ($T_{HW,in}$).

Figure 10 (*a-f*) show some examples of thermodynamic cycle displayed in the T-s diagram, obtained in four cases of operation with partial evaporation (*a-d*) and two cases with dry expansion (*e-f*). The selected cases can be considered as the boundary cycles of the analysis described in this paper, with temperature of the heat source equal to the minimum of 40 °C and to the maximum of 75 °C. The conditions represented in Figure 10 (*a-b*) refer to the operation with minimum value of vapour quality x_1 for the two heat source conditions, equal to 0.20 and to 0.73 for case *a* and case *b* (40 °C and 75 °C), respectively. Figure 10 (*c-d*) reports the cases of quality x_1 close to 1, thus with saturated vapour at the expander inlet. In case *c* (with $T_{HW,in} = 40\ °C$), the estimation of the enthalpy value at the expander outlet (point 2) indicates that the expansion occurs partly in the two-phase region and partly in dry condition, as the increment of entropy (thus the expansion losses) induces the fluid to superheat. Finally, Figure 10 (*e-f*) shows two conditions corresponding to DE operating mode at the same values of heat source

temperature of the PE cases, with a superheating degree of 3 K and 6.5 K for $T_{HW,in}$ equal to 40 °C and 75 °C, respectively.

In all the tested conditions in PE mode (such as those reported in the T-s diagrams of Figure 10 (*a-d*), the contribution of the recuperator is very limited, since the heat transferred from the hot side is only latent heat. Indeed, the average thermal power transferred in the recuperator ($\dot{Q}_{rec}$) is in the range 200-500 W, corresponding to a fraction between 1% and 5% of the evaporator thermal input ($\dot{Q}_{rec}/\dot{Q}_{eva}$). These values are far below the range of 2-5 kW occurring in case of dry expansion operation, leading to values of the ratio $\dot{Q}_{rec}/\dot{Q}_{eva}$ between 10% and 20%. The related temperature increment on the cold side of the recuperator (from point 6 to point 7 in Figure 2) is very low in PE mode, around 1-3 K, compared to the range of 10-25 K in the dry expansion mode. In a few cases with high values of x_1 (such as the case in Figure 10 (*c*)), the temperature rise in the preheating process increases up to 6-7 K, because the expansion ends with a slight superheating, and part of the heat transfer from the hot side of the recuperator involves sensible heat. According to what was expected, the use of the recuperator is not convenient when the expansion starts (and ends) in saturation conditions, as its contribution to the heat input is almost negligible and, on the other hand, it adds pressure losses to the fluid flow and increases system complexity. Therefore, a simple cycle without the recuperator is more suitable for an ORC system that is expected to operate with partial evaporation and wet expansion. If the system target is to work in both modes, depending on the external conditions, at least a bypass circuit should be provided for deviating the flow directly from the expander to the condenser when the recuperator is not useful, to avoid the pressure losses of the low-density vapour at the expander outlet. The bypass of the liquid (or cold) side of the recuperator is less crucial, because the fluid density is much higher and the flow speed, and hence the pressures losses, are reduced. In the conditions tested in this study, pressure losses of the low-pressure vapour between inlet and outlet of the recuperator are in the range 0.1 bar - 0.4 bar (between 1.5% and 5.5% of the inlet pressure), increasing with the mass flow rate and with the heat source temperature. In the T-s diagrams reported in Figure 10, pressure losses have been considered.

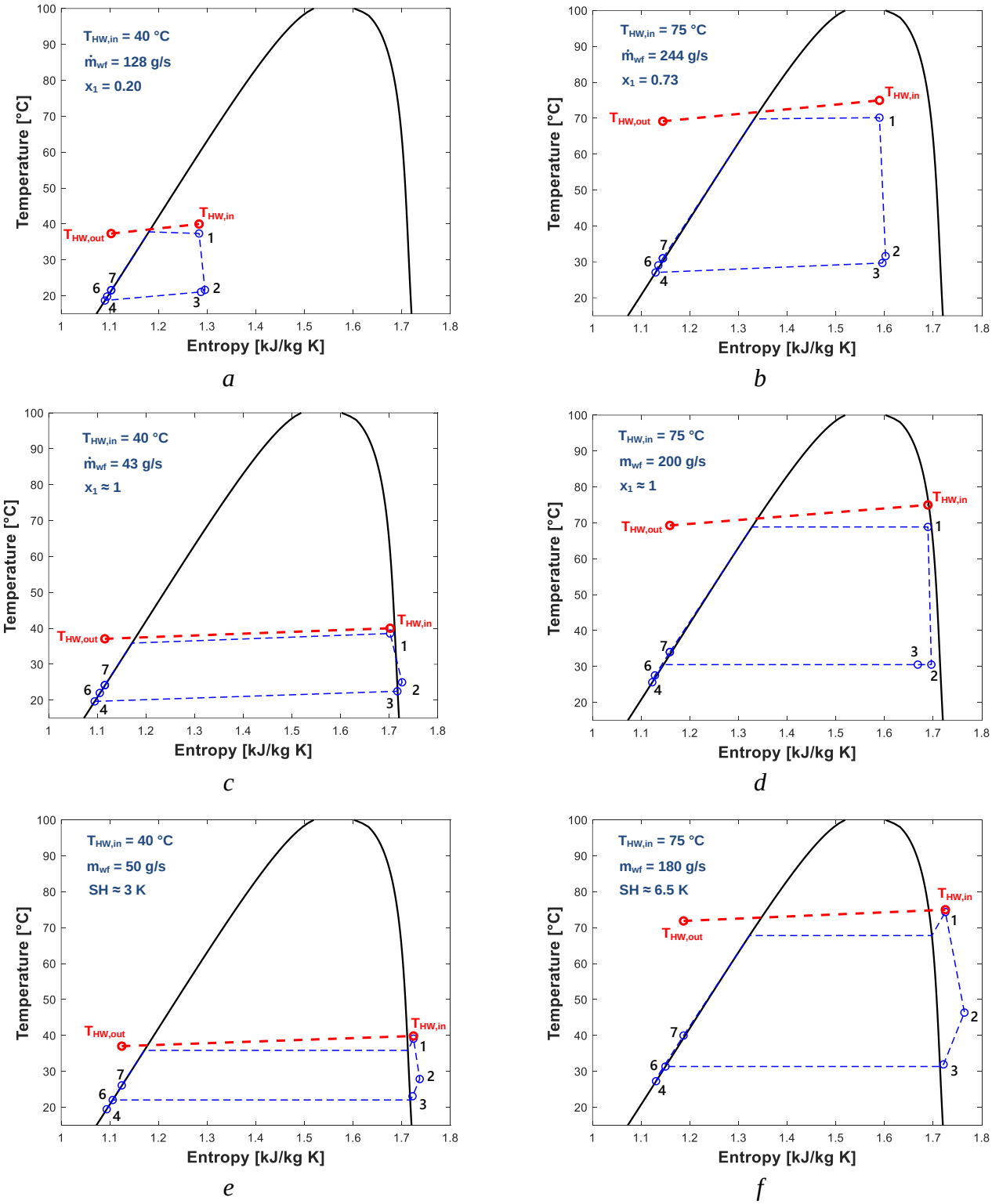

Figure 10 – temperature-entropy diagram for the boundary cycles: a) PE mode with minimum $T_{HW,in}$ and minimum x_1; b) PE mode with maximum $T_{HW,in}$ and minimum x_1; c) PE mode with minimum $T_{HW,in}$ and x_1 close to one; d) PE mode with maximum $T_{HW,in}$ and x_1 close to one; e) DE mode with minimum $T_{HW,in}$; e) DE mode with maximum $T_{HW,in}$.

4.2. Evaporator performance

The analysis of the variables related to the evaporator is fundamental to understand the operation of the ORC system with partial evaporation. One important outcome regards the trend of the thermal power transferred in the evaporator, $\dot{Q}_{eva}$. As shown in Figure 11, the heat exchanged in the evaporator depends mainly on the heat source temperature, while the effect of the mass flow rate of the working fluid is marginal. This is the opposite of what is observed in the experimental tests with dry expansion, in which the thermal power exchanged in evaporator and condenser is almost linear with the mass flow rate, with no significant effect related to the water temperature (see [21]). The different behaviour is connected to the trend of the working fluid specific enthalpy rise at the evaporator ($\Delta h_{eva} = h_1 - h_7$), reported in Figure 12. Indeed, in DE mode the value of Δh_{eva} remains in a relatively small range (between 140 kJ/kg and 170 kJ/kg) in all the conditions of heat source temperature and working fluid flow rate, while in PE operation Δh_{eva} decreases, at constant $T_{HW,in}$, by decreasing the quality x_1 (or by increasing $\dot{m}_{wf}$), within the range 30-160 kJ/kg. This reduction compensates the increment of the mass flow rate, resulting in limited variations of the transferred thermal power at constant temperature, as can be viewed in Figure 11. The minimum value of $\dot{Q}_{eva}$ is around 7 kW at $T_{HW,in} = 40\ °C$, while the maximum is slightly higher than 37 kW at $T_{HW,in} = 75\ °C$.

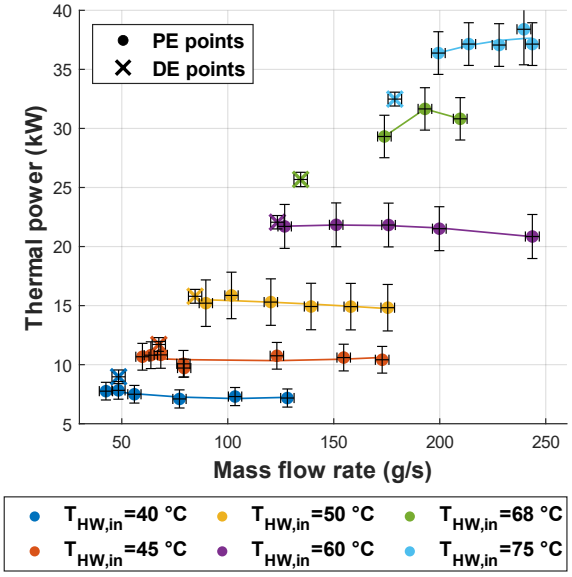

Figure 11 - evaporator thermal power versus mass flow rate, at different heat source temperatures.

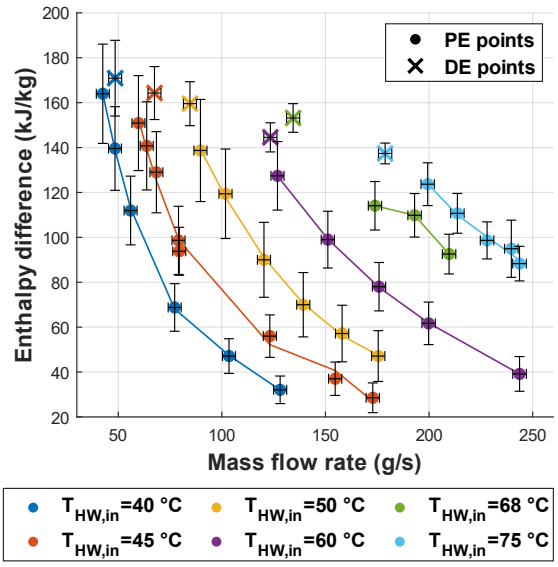

Figure 12 – specific enthalpy rise of the working fluid in the evaporator versus mass flow rate, at different heat source temperatures.

The performance of the evaporator is assessed using a definition of the heat transfer effectiveness (ε_{eva}), assuming that the plate evaporator can be analysed as a counter-flow heat exchanger with no thermal losses to the ambient. In the general case, the effectiveness of a heat exchanger is

computed as the ratio between the actual transferred thermal power and the maximum ideal heat that could be transferred with an infinite surface area ($\varepsilon = {\dot{Q}}/{\dot{Q}_{max}}$) [27].

Due to the occurrence of the phase change, the evaporator is virtually divided in two zones – namely the economizer (eco) and the vaporizer (vap) – in the direction of the flow inside the heat exchanger, and the effectiveness is calculated for each zone, according respectively to Equation (14) and Equation (15). The two equations derive from the same definition, but the final expressions differ as the effectiveness is calculated, for the economizer, from the organic fluid side, while for the vaporizer the water side is used, according to [28]. In Eq. (14), the term $h_{ev,L}$ is the enthalpy of the saturated liquid at the vaporization pressure, while h_7 is the enthalpy at the evaporator inlet. The symbol $h_{\tau pp=0}$ represents the liquid enthalpy calculated at a saturation temperature that is equal to the water temperature at the pinch point, $T_{HW,pp}$, in the ideal case of null pinch-point temperature difference. In Eq. (15), the effectiveness of the vaporizer zone is calculated using the terminal temperature difference, assuming constant values of water specific heat (c_{HW}) volume flow rate ($\dot{V}_{HW}$) and density (ρ_{HW}). A global effectiveness of the evaporator can be then calculated according to Equation (16), using the average values of the single zones effectiveness (ε_{eco} and ε_{vap}), weighted by the ideal thermal power of economizer and vaporizer zones.

$$\varepsilon_{eco} = \frac{\dot{Q}_{eco}}{\dot{Q}_{eco,max}} = \frac{\dot{m}_{wf} \cdot (h_{ev,L} - h_7)}{\dot{m}_{wf} \cdot (h_{\tau pp=0} - h_7)} = \frac{(h_{ev,L} - h_7)}{(h_{\tau pp=0} - h_7)} \tag{14}$$

$$\varepsilon_{vap} = \frac{\dot{Q}_{vap}}{\dot{Q}_{vap,max}} = \frac{\dot{V}_{HW} \cdot \rho_{HW} \cdot c_{HW} \cdot (T_{HW,in} - T_{HW,pp})}{\dot{V}_{HW} \cdot \rho_{HW} \cdot c_{HW} \cdot (T_{HW,in} - T_{vap})} = \frac{T_{HW,in} - T_{HW,pp}}{T_{HW,in} - T_{vap}} \tag{15}$$

$$\varepsilon_{eva} = \frac{\dot{Q}_{eco} + \dot{Q}_{vap}}{\dot{Q}_{eco,max} + \dot{Q}_{vap,max}} = \frac{\varepsilon_{eco} \cdot \dot{Q}_{eco,max} + \varepsilon_{vap} \cdot \dot{Q}_{vap,max}}{\dot{Q}_{eco,max} + \dot{Q}_{vap,max}} \tag{16}$$

The parameter UA, i.e. the product of the global heat transfer coefficient and the heat transfer surface, was evaluated for the economizer and the vaporizer according to Equations (17) and (18) [28].

$$UA_{\mathrm{eco}} = \frac{\dot{Q}_{\mathrm{eco}}}{LMTD_{eco}} = \frac{\dot{m}_{\mathrm{ORC}} \cdot (h_{ev,L} - h_7)}{(T_{HW,pp} - T_{vap}) - (T_{HW,out} - T_7)} \cdot \ln\left(\frac{T_{HW,pp} - T_{vap}}{T_{HW,out} - T_7}\right) \tag{17}$$

$$UA_{\mathrm{vap}} = \frac{\dot{Q}_{\mathrm{vap}}}{LMTD_{vap}} = \frac{\dot{m}_{\mathrm{ORC}} \cdot (h_1 - h_{ev,L})}{(T_{HW,in} - T_{vap}) - (T_{HW,pp} - T_{vap})} \cdot \ln\left(\frac{T_{HW,in} - T_{vap}}{T_{HW,pp} - T_{vap}}\right) \tag{18}$$

The trends of the effectiveness of the single zones and the global evaporator effectiveness are reported in Figure 13, as function of the mass flow rate of the working fluid. The economizer effectiveness (ε_{eco}, blue markers) keeps a quasi-constant trend, with values close to the unit in all the tested PE conditions. A slight decrease is observed at the lowest values of flow rate (below 100 g/s), still maintaining values above 0.85. The vaporizer effectiveness (ε_{vap}, red markers) is in the range 0.6-0.7 for most working conditions, with a relatively low decrease at low mass flow rate. Consequently, the global effectiveness (ε_{eva}, yellow markers) achieves highest values

slightly above 0.8, and an average range between 0.65 and 0.75 in the tested conditions. From a comparison of these values with those obtained in dry expansion operation (cross markers in Figure 13, more in detail in [21]), some considerations can be made.

First, the evaporator effectiveness with dry expansion varies in a wide range, increasing with the flow rate and decreasing with the heat source temperature. This trend is related to the value of the pinch point temperature difference, which is larger if the superheating degree is elevated, condition that corresponds in general to high temperature and low evaporation pressure (and low flow rate).

The substantial increment of ε_{eva}, whose values in dry conditions lie in the range 0.1-0.6, for the most part depends on the enhancement of the performance of the economizer and vaporizer zones, rather than on the absence of the superheater in PE conditions. Indeed, the superheating temperature, T_1, in DE operation is very close to the hot water inlet temperature, resulting in a superheater effectiveness close to 1. Moreover, due to the low superheating degree generally considered, the thermal power exchanged in the superheater is relatively small with respect to the heat transferred in economizer and vaporizer. The positive effect, indeed, is given by the increment of the economizer effectiveness, which is more evident at high mass flow rate, passing from values between 0.8 and 0.9 in DE conditions to an almost constant trend very close to 1 in PE mode. In addition, the fraction of the economizer transferred heat over the total evaporator thermal power rises significantly, achieving up to 50%, resulting in greater weight associated to the economizer in the calculation of the global effectiveness. The improvement of the vaporizer effectiveness is clear too, with average values around 0.65 in PE mode. Both the positive effects come from the strong reduction of the temperature difference between water and working fluid at the pinch point. The benefit of the PE operation on the economizer and vaporizer effectiveness results larger if the comparison is made with DE points characterized by high value of the superheating degree, since this condition involves an increment of the pinch point temperature difference.

The coefficient UA is displayed in Figure 14 for the economizer and the vaporizer, showing in both cases higher average values in PE conditions, especially with working fluid flow rate higher than 80 g/s. The economizer coefficient, UA_{eco}, increases almost linearly with $\dot{m}_{\mathrm{wf}}$, between 0.2 kW/K and 1.2 kW/K. The range of variation of the vaporizer coefficient, UA_{vap}, is between 3-5 kW/K for low mass flow rate, between 5 and 8 kW/K for medium and high values of $\dot{m}_{\mathrm{ORC}}$. It is also observed that values of UA_{vap} higher than 6 kW/K are obtained with vapour quality higher than 0.5.

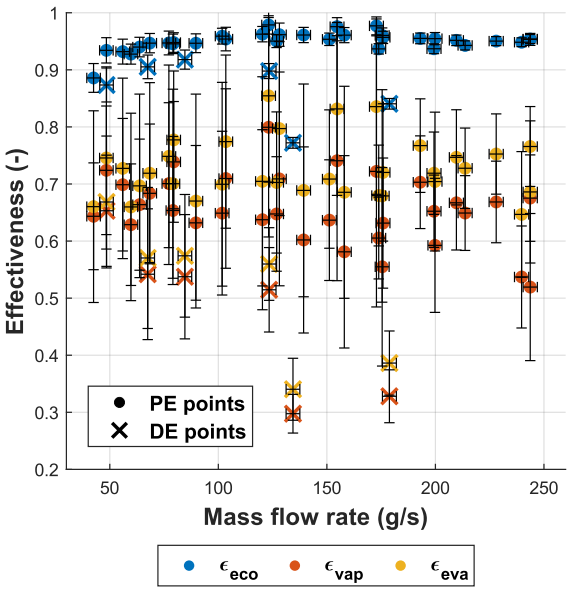

Figure 13 – effectiveness of the evaporation process, calculated according to Eq.s (14-16): ε_{eco}, ε_{vap} and ε_{eva} versus mass flow rate.

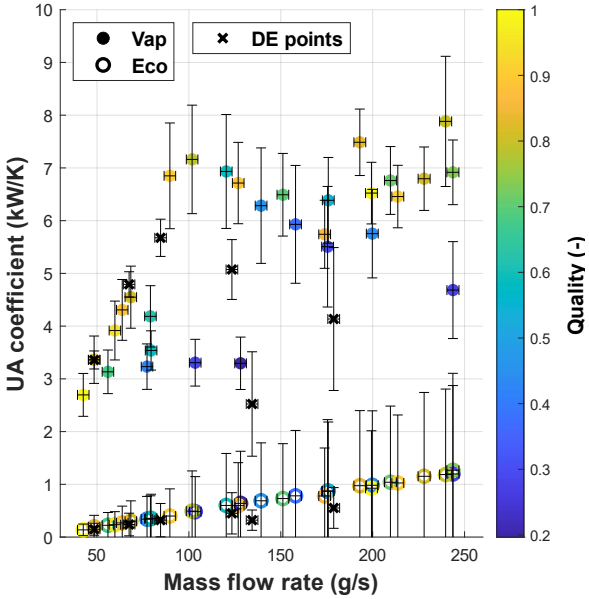

Figure 14 – UA values for the evaporator economizer and vaporizer versus mass flow rate in different test conditions. Colour bar indicates the corresponding vapour quality x_1.

Figure 15 reports the evaporator heat transfer diagram in two working conditions, obtained at the same temperature and flow rate of the hot water ($T_{HW,in} = 45\ °C$, $\dot{V}_{HW} = 1.0\ l/s$), and with different working fluid flow rate (60 g/s and 170 g/s). The case with lower value of $\dot{m}_{wf}$ (Figure 15*a*) is characterized by vapour quality at the expander inlet close to 1, and vaporization pressure equal to 10.5 bar. The low value of the pinch point temperature difference (≈ 1.5 K) leads to an improvement of both economizer and vaporizer effectiveness with respect to dry expansion. However, the ratio $\dot{Q}_{eco}/\dot{Q}_{eva}$ is limited (15%), and the global evaporator effectiveness results equal to 0.66. In Figure 15*b*, the value of τ_{pp} is even lower (below 1 K), resulting in larger improvement of the single zones effectiveness. Moreover, the economizer thermal power represents more than half the total evaporator thermal power. The effect is a substantial improvement of the global effectiveness of the evaporator, which achieves a value close to 0.84.

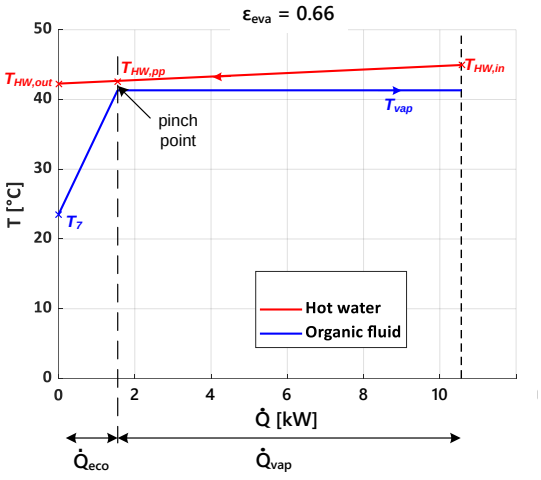

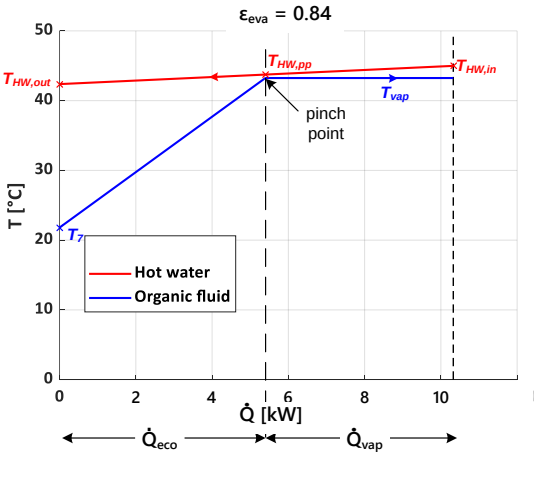

a) *b)*

Figure 15 – heat transfer diagram ($T, \dot{Q}_{eva}$) for the evaporator; a) $T_{Hin} = 45\ °C,\ \dot{m}_{ORC} = 60\ g/s$; b) $T_{Hin} = 45\ °C,\ \dot{m}_{ORC} = 170\ g/s$.

4.3. Expander and pump performance

From the analysis of Figure 16 (showing the expander electric power ($\dot{W}_{exp,el}$) versus the working fluid mass flow rate, for different values of the heat source temperature), it is clear that also the expander performance follows a different trend in PE mode with respect to the dry expansion operation. At constant hot water temperature, the electric power decreases with the increment of the mass flow rate, due to the reduction of the vapour quality at the expander inlet, which causes lower amount of vapour to expand inside the cylinders. The maximum values of $\dot{W}_{exp,el}$ resulted around 130 W with $T_{HW,in} = 40\ °C$, close to 580 W at 60 °C and to 1160 W at 75 °C.

The trends of the expander rotational speed (N_{exp}, Figure 17) are similar to those of the power output. The reduction of N_{exp} with the mass flow rate (at constant $T_{HW,in}$) can be correlated to the reduction of the working fluid density at the expander inlet, which leads to lower volume flow rate entering the cylinders. The range of variation of N_{exp} is 190-240 rpm at 40 °C, 400-500 rpm at 60 °C and 700-850 rpm at 75 °C.

The expander filling factor (*FF*) is reported in Figure 18, showing a general decreasing trend with the mass flow rate of the working fluid and with the heat source temperature. The highest values in PE mode (0.9-1.0) are obtained with temperatures up to 45 °C, while the average *FF* with $T_{HW,in}$ from 50 °C to 68 °C is in the range 0.7-0.8. The minimum average value of 0.6 is observed with a temperature equal to 75 °C. Compared to the DE case, a general improvement of the filling factor is observed in PE mode. This is most likely due to the lower expander speed of the PE points at the same $T_{HW,in}$, as it was observed also in DE operation that the filling factor decreases in general with the increment of the expander speed [22].

It is interesting to visualize the behaviour of the expander total efficiency (η_{exp}), evaluated according to Eq. (9), versus the expander rotational speed (Figure 19). The value of η_{exp} increases, at constant $T_{HW,in}$, with the expander speed increment. Increasing the temperature, the average value of η_{exp} decreases, being in the range 0.30-0.38 at 40 °C, between 0.26-0.34 at 60 °C and between 0.26 and 0.31 at 75 °C. In PE conditions, a lower expander speed is related to high mass flow rate (at constant $T_{HW,in}$, see Figure 17) and therefore to a lower vapour quality x_1. The reduction of the vapour quality is associated to a penalization of the efficiency, increasing the expansion losses and lowering the power output.

There is in general a penalization on the expander performance in case of wet expansion compared to the DE operation. The penalization is stronger for values of the vapour quality lower than 0.5, and for high heat source temperature, especially at 75 °C, at which the efficiency remains lower than 30% for any value of the quality x_1. At constant temperature, the reduction of the efficiency between the DE point and the PE point at highest vapour quality is limited in most cases (within 5 percentage points). This result suggests that the working conditions characterized by high value of the vapour quality (higher than 0.8) may involve limited penalization on the

expander performance. This aspect can be useful for example in a system designed for DE operation in case it is forced to work in PE mode.
On the other hand, the expander installed in this test bench has been proven to be not optimized, in terms of filling performance, also in DE operation, as highlighted in a previous study conducted on the same test bench [29]. The study regarded a modelling analysis aimed at optimizing the expander intake stroke ratio, depending on the inlet conditions of the working fluid. The modelling approach could be applied, after opportune adaptation, also to the expander working in wet conditions, with the purpose of designing variable-timing intake valves for assuring the maximization of the filling performance.
Another line of investigation for improving the expander performance might be the configuration with variable displacement, with the possibility of regulating the built-in volume ratio to adapt the expander internal volume to the change of inlet volumetric flow in PE conditions.

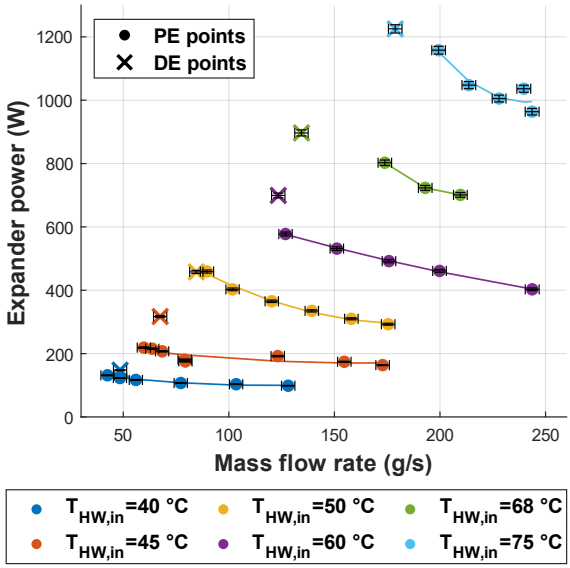

Figure 16 – electrical power produced by the expander versus mass flow rate, at different heat source temperatures.

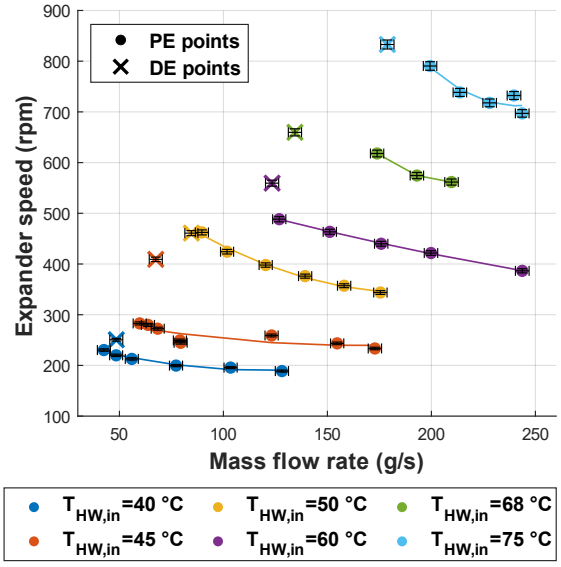

Figure 17 – expander speed versus mass flow rate, at different heat source temperatures.

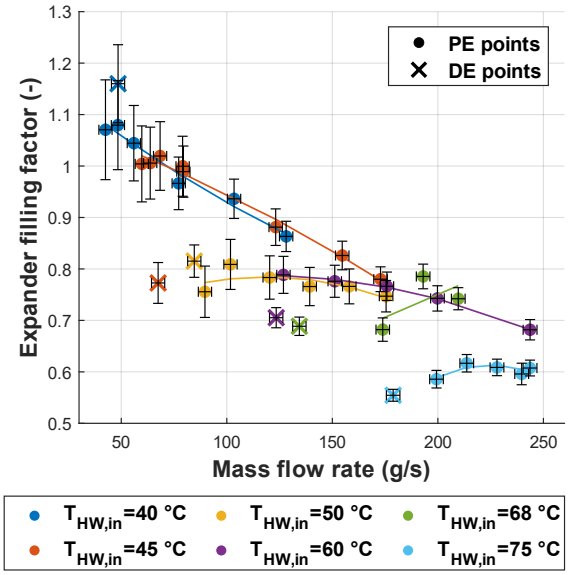

Figure 18 – expander filling factor versus mass flow rate, at different heat source temperatures.

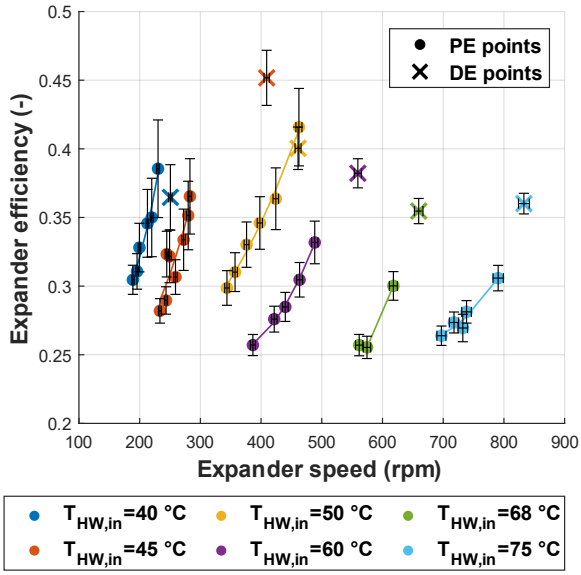

Figure 19 – expander total efficiency versus expander speed, at different heat source temperatures.

The analysis of the results related to the feed-pump highlighted that the operation in PE mode leads to better performance of the machine, in terms of volumetric efficiency and total efficiency, compared to the PE operation. The volumetric efficiency (η_{vol}), as shown in Figure 20, increases with the mass flow rate, and achieves the highest values (around 73%) at the minimum quality x_1, for each value of the heat source temperature up to 60 °C. At the highest temperatures (68 °C and 75 °C, green and light blue markers, respectively), the maximum η_{vol} is around 65%. In case of dry expansion, the maximum value of pump volumetric efficiency that has been registered is around 60%, while the minimum is below 45%.

The total efficiency of the feed pump (η_{pump}) is presented in Figure 21, showing a general increasing trend versus the mass flow rate of the working fluid, with the curves that are shifted above by increasing the heat source temperature. The maximum value of η_{pump} in PE conditions is around 37%, substantially higher than the maximum efficiency obtained in dry expansion condition, close to 30%. At constant heat source temperature, the improvement of η_{pump} is mainly due to the higher mass flow rate that is achieved in PE conditions, as η_{pump} increases almost linearly with the increment of $\dot{m}_{ORC}$.

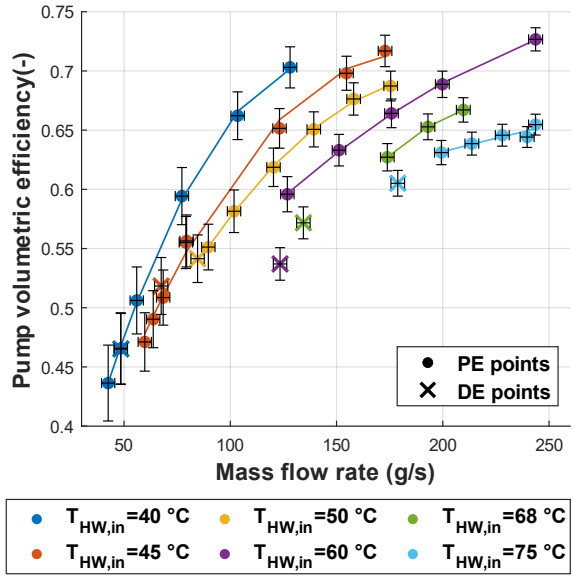

Figure 20 – pump volumetric efficiency versus mass flow rate, at different heat source temperatures.

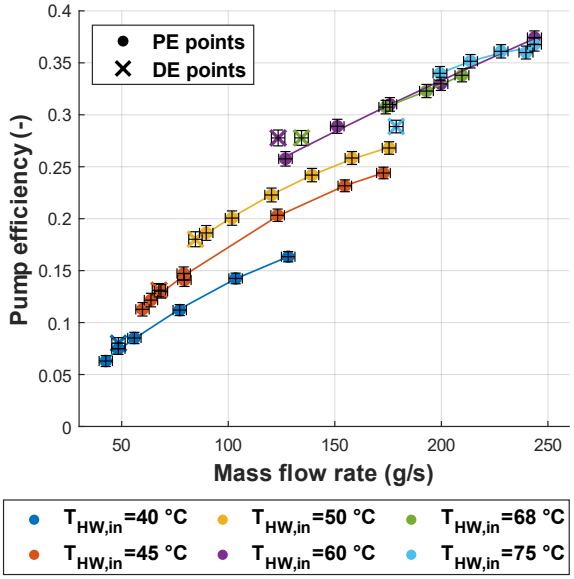

Figure 21 – pump total efficiency versus mass flow rate, at different heat source temperatures.

4.4. System efficiency

The very small size of the power plant, together with the relatively low performance of the machines and with the fact that the system is not optimized for working in partial evaporation mode, determines a remarkable impact of the feed pump consumption to the net power output, even though the pump total efficiency has been improved by the PE operation. This aspect is evident at the lowest tested power output, which corresponds, according to Figure 16, also to the lowest values of the heat source temperature. This is confirmed by the trend of the back work ratio (*BWR*) in Figure 22, which shows that the pump absorbs more power than that produced by the expander when the temperature is below 45 °C, in all the conditions of working fluid flow rate. The best condition (with $BWR \approx 50\%$) is obtained at quality close to 1 (hence with minimum flow rate), with temperature from 50 °C to 75 °C.

The overall performance, displayed in terms of second law efficiency (η_{II}, Eq. (7)), is reported in Figure 23. The figure includes only the points characterized by a positive value of η_{II}. At constant heat source temperature, the efficiency decreases with the increment of the working fluid mass flow rate. The average value of η_{II} is rather scarce, since it results below 10% in most PE conditions, with peaks lower than 15%. It is visible that also in DE mode the impact of the feed-pump consumption determines low values of the second law efficiency, in the range between 10% and 15 %. With a heat source temperature of 40 °C, no net power is produced by the micro-ORC system, neither in DE mode.

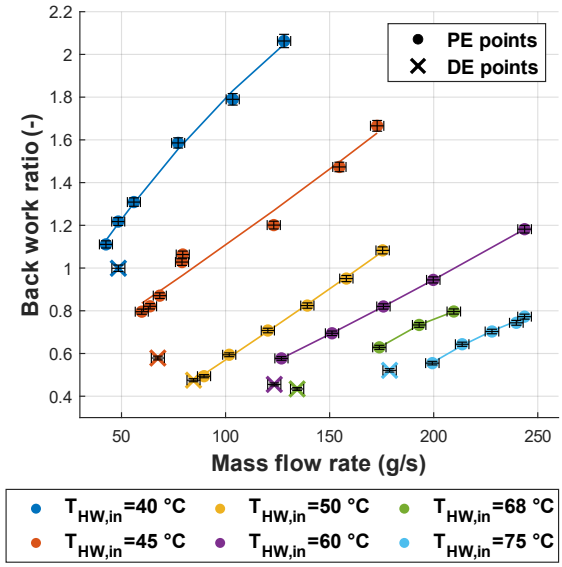

Figure 22 – back work ratio (BWR) versus mass flow rate, at different heat source temperatures.

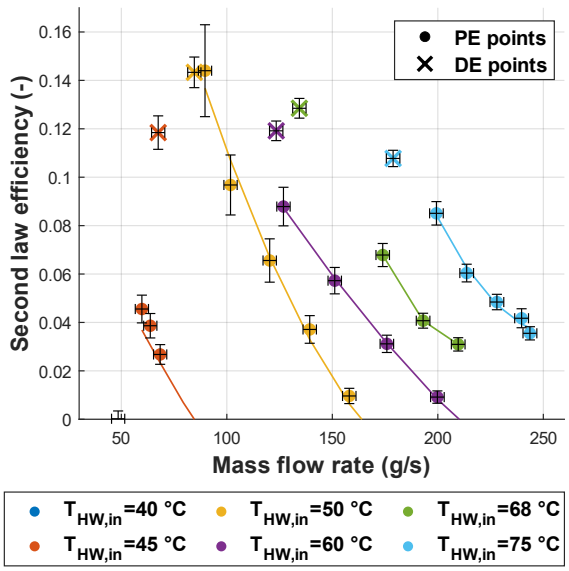

Figure 23 – second law efficiency versus mass flow rate, at different heat source temperatures.

Figure 24 collects the relative variations of the key performance indexes in PE operation with respect to the dry expansion case. The selected indexes are the expander power ($\dot{W}_{exp,el}$), efficiency (η_{exp}) and filling factor (FF), the pump total and volumetric efficiency (η_p and $\eta_{vol,p}$), the evaporator effectiveness (ε_{eva}), the back work ratio (BWR) and the second law efficiency (η_{II}). For the PE mode, the relative variation is computed taking the most favourable conditions, meaning the highest value obtained for all the variables except for the *BWR*, for which the minimum value is considered as the best performance. A positive variation indicates that the value of the variable is higher in PE mode.

The figure highlights that the pump efficiency is improved for all the tested values of heat source temperature, with a minimum increment of 25% for $T_{HW,in} = 75\ °C$, and a maximum slightly above 100%, for $T_{HW,in} = 40\ °C$. It must be highlighted that the pump efficiency is in general low at low mass flow rate, conditions that characterizes the DE operation at low heat source temperature. The relative improvement of the pump volumetric efficiency is in the range between 8% and 51%, increasing as the heat source temperature is reduced. Also, the evaporator effectiveness results significantly higher in all the tested conditions, with a relative variation from 20% up to 125%. The expander power output and total efficiency are lower in the PE mode in most conditions of the heat source, with a maximum relative reduction around -23% and -19%, respectively. On the contrary, for the expander filling factor (*FF*) an improvement up to 32% is observed in the PE mode. The back work ratio (*BWR*) is always higher in the PE points, with a relative increment between 4% and 37%. The reason of this penalization, considering that the pump presents better efficiency – increasing with the mass flow rate – in most operating conditions in PE mode (see Figure 21), is that the pump consumption also increases with the mass flow rate, while the expander power decreases (see Figure 16). The second law efficiency (η_{II}) is penalized in PE mode in all the considered conditions, due to the effect of *BWR*, but also to the strongly reduced contribution of the recuperator to the required thermal input, compared to the dry expansion operation.

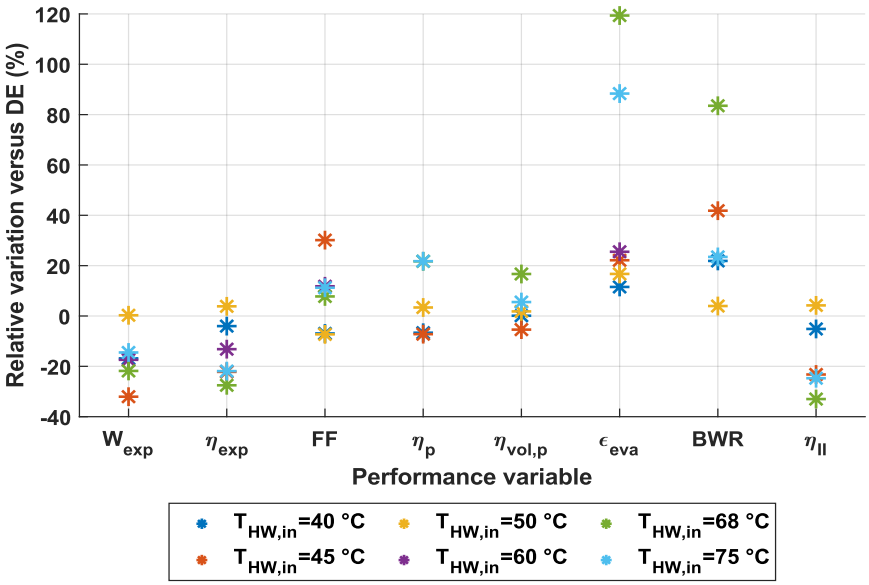

Figure 24 – relative variation for the key performance variables. A positive variation means that the index is higher in the PE mode than in the DE mode.

4.5. Overall discussion

Some concluding remarks can be provided considering the overall results. One scope of the experiments was to test the cycle, and in particular the piston expander, under severe off-design conditions. Within the entire set of experimental conditions presented in this paper, the cycle operation was stable and the expander produced electrical power continuously. It was possible to achieve the lowest values of the vapour quality (in the range 0.2-0.3) with a temperature of the heat source from 40 °C to 60 °C and high mass flow rate of the working fluid. The minimum achievable quality with temperatures of 68 °C and 75 °C is higher than 0.6, due to the limit of this specific test bench.

In all the cases, the overall performance of the system decreases by decreasing the vapour quality. For this reason, the most interesting range of working condition, at the different heat source temperatures, is that with vapour quality between 0.8 and 1. Indeed, the improvement of the evaporator performance is mainly caused by the absence of superheating, while the reduction of the vapour quality does not provoke any significant further increment of the effectiveness or of the heat transfer coefficient.

It must be pointed out that the performance of the system under investigation is scarce, especially if the temperature of the heat source is lower than 60 °C, also in dry expansion conditions. The application of the partial evaporation in this range of temperature may be of interest in the view of exploiting ultra-low temperature waste heat.

A system specifically designed for working in PE mode, thus with optimized expander and sizes of the components, may benefit from the improvement of the evaporator performance and from the removal (or by-pass) of the recuperator, which would involve a simpler and less expensive system and lower pressure losses. The possibility of adjusting some expander parameters depending on the working conditions, such as the valve timing and/or the displacement, can help to maintain acceptable expander performance. A very important issue remains the feed-pump

consumption, which in ORC systems of such scale is considerable, especially at low heat source temperature. A proper redesign of the pump, including the electric motor, should be performed to reduce the back work ratio to acceptable values (i.e. below 30%) and increase the overall conversion efficiency.
The results suggest also that the partial evaporation may be employed as off-design condition in ORC systems that are designed for dry expansion. This control solution is more suitable in systems working with low superheating degree, and with temperature of the heat source that is expected to change quite frequently. To make an example, with a certain reduction of the heat source temperature from the design value, the partial evaporation can be adopted as regulation strategy, with the aim of reducing the off-design performance penalization. Indeed, if the system is regulated in DE mode maintaining constant the superheating degree, the evaporation temperature and pressure must decrease by reducing the mass flow rate, which will cause a penalization of the expander work and power output. On the other hand, switching to PE mode could allow to keep the evaporation pressure at higher level than in the previous case (hence higher expansion ratio), due to the lower pinch point temperature difference compared to DE. Moreover, if the vapour quality is maintained high, the penalization of the expander efficiency is limited, and there is a compensation to the overall efficiency due to the improvement of the evaporator performance. Also in this case, the regulation of the parameters that maintain the optimum filling process is fundamental for maximizing the expander performance varying the operating conditions.

5. Conclusion

This paper provides for a comprehensive experimental analysis of a micro-ORC system for low-temperature heat recovery, operated with partial evaporation (PE-ORC) and wet expansion. The system was developed for working with dry expansion, hence the presented results are related to operating conditions that can be considered strongly off-design. Nevertheless, the micro-ORC test bench has proven to be effective for the understanding of the behaviour of its main components (expander, pump and heat exchangers), and of the potential application of the PE operating mode in the energy conversion from very low temperature heat sources (from 40 °C to 75 °C).
The aim of the study was to demonstrate the capability of the micro-ORC to work in PE mode, highlighting the difference with respect to the regular operation with dry expansion (DE mode), especially regarding the trend and influence of each main variable.
The main outcomes are summarized below:

- in PE mode, the vaporization pressure is mostly influenced by the heat source temperature, while the effect of the working fluid mass flow rate is minimum. At constant temperature, the increment of the mass flow causes the reduction of the vapour quality at the expander inlet. The minimum achieved vapour quality was 0.2 at the minimum values of the heat source temperature (equal to 40 °C and 45 °C).

- The condensation pressure, which is mainly related to the cold sink conditions, remains constant varying the flow rate of the working fluid.
- The performance of the organic fluid pump in PE conditions is characterized by a substantial improvement compared to the dry expansion, with an important increment of both the volumetric efficiency and the total efficiency, whose maximum value is close to 37% (against a maximum below 30% in DE).
- The performance of the evaporator is improved significantly in PE conditions: the heat transfer effectiveness in the vaporizer and in the economizer zone increases, resulting in a relevant enhancement of the global effectiveness of the evaporator, with a relative variation with respect to dry expansion mode up to +125%. The temperature difference between the hot water and the organic fluid at the pinch point is reduced to the smallest value (1-2 K), for all the conditions in partial evaporation mode.
- The contribution of the recuperator to the thermal input is minimal, since the heat transferred from the hot side is only latent heat. The temperature rise on the cold side of the heat exchanger is only of few degrees, against a value between 10 K and 25 K obtainable in DE mode.
- The maximum electrical power produced by the expander resulted close to 1.2 kW, obtained with a temperature of the heat source of 75 °C and a vapour quality at the expander inlet close to one.
- The volumetric expander adopted in this test bench is suitable for the wet expansion, although the performance should be improved. If the vapour quality is reduced at constant heat source temperature, the expander power output decreases; the penalization is less important at the lower temperature of the heat source. The expander efficiency is penalized in most of the tested condition, especially at the highest values of the heat source temperature (from 60 °C), with relative variation compared to DE mode up to -19%. At vapour quality above 0.8, the reduction of the expander efficiency with respect to the dry expansion is smaller.

- In some of the PE working conditions, the back work ratio (*BWR*) results higher than the unit, with peaks close to 2. It must be said that, also in the DE mode, the minimum value of *BWR* is around 0.5, with peaks close to 1.

In conclusion, the reduction of the pinch point temperature difference, characterizing the PE operating mode, assures better utilization of the heat source compared to dry expansion, with a significant increment of the effectiveness of the evaporator. Moreover, in the case of this study the pump performance benefits from the PE mode. The main challenge to be addressed regards the performance of the expander, which is strongly penalized by the wet expansion. The machine used for this investigation demonstrated to be able to work with wet expansion, but the efficiency needs to be improved. A possible improvement action could be the optimization of the expander valve timing, aimed at increasing the filling performance within specific conditions of vapour quality at the expander inlet.

References

[1] Bianchi, G., McGinty, R., Oliver, D., Brightman, D., Zaher, O., Tassou, S.A., Miller, J., Jouhara, H., 2017. Development and analysis of a packaged Trilateral Flash Cycle system for low grade heat to power conversion applications. Thermal Science and Engineering Progress 4, 113–121. https://doi.org/10.1016/j.tsep.2017.09.009

[2] Forman, C., Muritala, I.K., Pardemann, R., Meyer, B., 2016. Estimating the global waste heat potential. Renewable and Sustainable Energy Reviews 57, 1568–1579. https://doi.org/10.1016/j.rser.2015.12.192

[3] Lemort, V., Legros, A., 2017. Positive displacement expanders for Organic Rankine Cycle systems, in: Organic Rankine Cycle (ORC) Power Systems. Elsevier, pp. 361–396. https://doi.org/10.1016/B978-0-08-100510-1.00012-0

[4] Tammone, C., Pili, R., Indrehus, S., Haglind, F., 2021. TECHNO-ECONOMIC ANALYSIS OF PARTIAL EVAPORATION ORGANIC RANKINE CYCLE SYSTEMS FOR GEOTHERMAL APPLICATIONS 10.

[5] Smith, I. K., 1993, Development of the trilateral flash cycle system Part 1 : fundamental considerations, Proceedings of the Institution of Mechanical Engineers, Part A: Journal of Power and Energy, vol. 207, no. 3, p. 179–194.

[6] Fischer, J., 2011. Comparison of trilateral cycles and organic Rankine cycles. Energy 36, 6208–6219. https://doi.org/10.1016/j.energy.2011.07.041

[7] Quoilin, S., Broek, M.V.D., Declaye, S., Dewallef, P., Lemort, V., 2013. Techno-economic survey of Organic Rankine Cycle (ORC) systems. Renewable and Sustainable Energy Reviews 22, 168–186. https://doi.org/10.1016/j.rser.2013.01.028.

[8] Cipollone, R., Bianchi, G., Di Bartolomeo, M., Di Battista, D., Fatigati, F., 2017. Low grade thermal recovery based on trilateral flash cycles using recent pure fluids and mixtures. Energy Procedia 123, 289–296. https://doi.org/10.1016/j.egypro.2017.07.246

[9] Lai, K.-Y., Lee, Y.-T., Chen, M.-R., Liu, Y.-H., 2019. Comparison of the Trilateral Flash Cycle and Rankine Cycle with Organic Fluid Using the Pinch Point Temperature. Entropy 21, 1197. https://doi.org/10.3390/e21121197

[10] McGinty, R., Bianchi, G., Zaher, O., Woolass, S., Oliver, D., Williams, C., Miller, J., 2017. Techno-economic survey and design of a pilot test rig for a trilateral flash cycle system in a steel production plant. Energy Procedia 123, 281–288. https://doi.org/10.1016/j.egypro.2017.07.242

[11] Skiadopoulos, A., van Heule, X., Kosmadakis, G., Manolakos, D., Paepe, M.D., Lecompte, S., 2021. THERMODYNAMIC LOW-ORDER MODEL FOR THE SIMULATION OF TWO- PHASE EXPANSION IN A TFC UNIT 10.

[12] Wang, Q., Wu, W., He, Z., Ziviani, D., 2019. Analysis of the intake process and its influence on the performance of a two-phase reciprocating expander. Applied Thermal Engineering 160, 113943. https://doi.org/10.1016/j.applthermaleng.2019.113943

[13] White, M.T., 2021. Cycle and turbine optimisation for an ORC operating with two-phase expansion. Applied Thermal Engineering 192, 116852. https://doi.org/10.1016/j.applthermaleng.2021.116852

[14] Steidel, R.F., H. and Flower, J.E. (1982). Performance Characteristics of the Lysholm Engine as Tested for Geothermal Applications in the Imperial Valley. Trans ASME, Journal of Eng for Power, Vol. 104, pp. 231-240.

[15] I.K. Smith, N. Stosic, C.A. Aldis, Development of the trilateral flash cycle system Part 3. The design of high-efficiency two-phase screw ex panders, J. Power Energy 210 (1996) 75–93.

[16] Öhman, H., Lundqvist, P., 2013. Experimental investigation of a Lysholm Turbine operating with superheated, saturated and 2-phase inlet conditions. Applied Thermal Engineering 50, 1211–1218. https://doi.org/10.1016/j.applthermaleng.2012.08.035

[17] Iqbal, A., 2020. Experimental study on the prospect of low-temperature heat to power generation using Trilateral Flash Cycle (TFC). Applied Thermal Engineering 13.

[18] Dawo, F., Buhr, J., Wieland, C., Spliethoff, H., 2021. Experimental investigation of the partial evaporated organic Rankine cycle for various heat source conditions 9. Proceedings of the 6th International Seminar on ORC Power Systems 11 - 13 September 2021, Munich, Germany.

[19] Kanno, H., Shikazono, N., 2015. Experimental and modeling study on adiabatic two-phase expansion in a cylinder. International Journal of Heat and Mass Transfer 86, 755–763. https://doi.org/10.1016/j.ijheatmasstransfer.2015.02.059

[20] Löffler, M.K., 2008. Flash Evaporation in Cyclones. Chem. Eng. Technol. 31, 1062–1065. https://doi.org/10.1002/ceat.200700470

[21] Ottaviano, S., 2021. Test bench development, experimental analysis and modelling of micro-organic Rankine cycle for low-grade heat recovery. Doctoral Thesis. https://doi.org/10.48676/UNIBO/AMSDOTTORATO/9784

[22] Bianchi, M., Branchini, L., Casari, N., De Pascale, A., Melino, F., Ottaviano, S., Pinelli, M., Spina, P.R., Suman, A., 2019. Experimental analysis of a micro-ORC driven by piston expander for low-grade heat recovery. Applied Thermal Engineering 148, 1278–1291. https://doi.org/10.1016/j.applthermaleng.2018.12.019

[23] Bianchi, M., Branchini, L., Casari, N., Pascale, A.D., Fadiga, E., Melino, F., Ottaviano, S., Peretto, A., Pinelli, M., Spina, P.R., Suman, A., 2019. Uncertainty quantification of performance parameters in a small scale ORC test rig. Proceedings of the 5th International Seminar on ORC Power Systems 9 - 11 September 2019, Athens, Greece.

[24] Zampieri G. "CLOSED-CYCLE PLANT." U.S. Patent No. 20,160,032,786. 4 Feb. 2016.

[25] I.H. Bell, J. Wronski, S. Quoilin, V. Lemort, Pure and pseudo-pure fluid thermophysical property evaluation and the open-source thermophysical property library CoolProp, Ind. Eng. Chem. Res 53 (6) (2014) 498–508, https://doi.org/10.1021/ie4033999

[26] Bianchi, M., Branchini, L., De Pascale, A., Orlandini, V., Ottaviano, S., Peretto, A., Melino, F., Pinelli, M., Spina, P.R., Suman, A., 2017. Experimental Investigation with Steady-State Detection in a Micro-ORC Test Bench. Energy Procedia 126, 469–476. https://doi.org/10.1016/j.egypro.2017.08.222.

[27] W. C. Reynolds and H. C. Perkins, ENGINEERING THERMODYNAMICS, Second. McGraw-Hill, Inc., 1977.

[28] F. P. Incropera, D. P. Dewitt, T. L. Bergman, and A. S. Lavine, Introduction to Heat Transfer, Fifth. John Wiley & Sons, Inc., 2007.

[29] Bianchi, M., Branchini, L., De Pascale, A., Melino, F., Ottaviano, S., Peretto, A., Torricelli, N., 2020. Replacement of R134a with low-GWP fluids in a kW-size reciprocating piston expander: Performance prediction and design optimization. Energy 206, 118174. https://doi.org/10.1016/j.energy.2020.118174

Appendix

Average measured results with uncertainty ranges.

$\dot{m}_{ORC}$ [g/s]	p_1 [bar]	p_2 [bar]	p_4 [bar]	p_6 [bar]	p_7 [bar]	T_1 [°C]	T_2 [°C]	T_4 [°C]	T_6 [°C]	T_7 [°C]	T_{HWin} [°C]	T_{HWout} [°C]	$\dot{V}_{HW}$ [l/s]	T_{CWin} [°C]	T_{CWout} [°C]	$\dot{V}_{CW}$ [l/s]	$\dot{W}_{exp}$ [W]	N_{exp} [rpm]	$\dot{W}_p$ [W]	N_p [rpm]
77.2 ± 3.13	9.404 ± 0.012	6.066 ± 0.006	5.994 ± 0.007	9.485 ± 0.007	9.506 ± 0.015	36.96 ± 0.20	21.65 ± 0.19	18.63 ± 0.16	20.21 ± 0.21	21.58 ± 0.18	39.95 ± 0.20	37.33 ± 0.20	0.648 ± 0.003	14.36 ± 0.20	15.87 ± 0.20	1.156 ± 0.003	107.1 ± 1.14	199.6 ± 2.13	169.8 ± 1.81	98.4 ± 1.05
56.0 ± 3.13	9.253 ± 0.012	6.091 ± 0.006	6.037 ± 0.007	9.346 ± 0.007	9.327 ± 0.015	36.59 ± 0.20	21.99 ± 0.19	19.48 ± 0.16	21.56 ± 0.21	22.02 ± 0.18	39.96 ± 0.20	37.12 ± 0.20	0.631 ± 0.003	15.73 ± 0.20	17.29 ± 0.20	1.181 ± 0.003	116.8 ± 1.25	212.8 ± 2.27	152.9 ± 1.63	83.7 ± 0.89
128.1 ± 3.16	9.581 ± 0.012	6.092 ± 0.006	5.993 ± 0.007	9.687 ± 0.007	9.669 ± 0.015	37.35 ± 0.20	21.64 ± 0.19	18.69 ± 0.16	19.81 ± 0.21	21.56 ± 0.18	39.98 ± 0.20	37.33 ± 0.20	0.648 ± 0.003	14.39 ± 0.20	15.93 ± 0.20	1.152 ± 0.003	98.5 ± 1.14	188.9 ± 2.02	203.2 ± 2.17	138.3 ± 1.48
42.5 ± 3.12	9.090 ± 0.012	6.116 ± 0.006	6.089 ± 0.007	9.143 ± 0.007	9.133 ± 0.015	38.56 ± 0.20	24.98 ± 0.19	19.66 ± 0.16	22.00 ± 0.21	24.18 ± 0.18	40.03 ± 0.20	37.09 ± 0.20	0.631 ± 0.003	15.77 ± 0.20	17.46 ± 0.20	1.103 ± 0.003	131.5 ± 1.40	230.3 ± 2.46	146.0 ± 1.56	73.5 ± 0.79
48.4 ± 3.12	9.238 ± 0.012	6.113 ± 0.006	6.065 ± 0.007	9.318 ± 0.007	9.306 ± 0.015	36.54 ± 0.20	22.12 ± 0.19	19.56 ± 0.16	21.83 ± 0.21	22.14 ± 0.18	40.05 ± 0.20	37.08 ± 0.20	0.631 ± 0.003	15.74 ± 0.20	17.39 ± 0.20	1.154 ± 0.003	122.8 ± 1.31	219.9 ± 2.35	149.5 ± 1.60	78.6 ± 0.84
103.4 ± 3.14	9.498 ± 0.012	6.091 ± 0.006	6.006 ± 0.007	9.625 ± 0.007	9.592 ± 0.015	37.16 ± 0.20	21.69 ± 0.19	18.75 ± 0.16	20.01 ± 0.21	21.64 ± 0.18	40.05 ± 0.20	37.36 ± 0.20	0.648 ± 0.003	14.40 ± 0.20	15.96 ± 0.20	1.154 ± 0.003	103.3 ± 1.10	195.7 ± 2.09	184.9 ± 1.98	118.5 ± 1.27
79.1 ± 3.14	10.697 ± 0.012	6.313 ± 0.006	6.240 ± 0.007	10.790 ± 0.007	10.780 ± 0.015	42.00 ± 0.20	23.16 ± 0.19	20.70 ± 0.16	22.11 ± 0.21	23.11 ± 0.18	44.94 ± 0.20	42.42 ± 0.20	0.957 ± 0.003	15.76 ± 0.20	17.91 ± 0.20	1.105 ± 0.003	181.0 ± 1.93	249.3 ± 2.66	186.1 ± 1.99	108.2 ± 1.16
59.7 ± 3.13	10.529 ± 0.012	6.272 ± 0.006	6.222 ± 0.007	10.607 ± 0.007	10.601 ± 0.015	41.86 ± 0.20	23.57 ± 0.19	20.52 ± 0.16	22.53 ± 0.21	23.51 ± 0.18	44.94 ± 0.20	42.27 ± 0.20	0.957 ± 0.003	15.69 ± 0.20	17.69 ± 0.20	1.246 ± 0.003	218.8 ± 1.34	282.8 ± 3.02	174.1 ± 1.86	96.0 ± 1.03
172.8 ± 3.20	11.079 ± 0.012	6.150 ± 0.006	6.008 ± 0.007	11.187 ± 0.007	11.171 ± 0.015	42.84 ± 0.20	21.96 ± 0.19	19.00 ± 0.16	20.12 ± 0.21	21.81 ± 0.18	44.99 ± 0.20	42.37 ± 0.20	0.954 ± 0.003	14.24 ± 0.20	15.86 ± 0.20	1.553 ± 0.003	163.6 ± 1.75	233.4 ± 2.49	272.5 ± 2.91	183.3 ± 1.96
68.4 ± 3.13	10.656 ± 0.012	6.236 ± 0.006	6.171 ± 0.007	10.736 ± 0.007	10.725 ± 0.015	41.92 ± 0.20	22.83 ± 0.19	20.27 ± 0.16	22.11 ± 0.21	22.76 ± 0.18	45.03 ± 0.20	42.33 ± 0.20	0.957 ± 0.003	15.67 ± 0.20	17.54 ± 0.20	1.346 ± 0.003	207.1 ± 2.21	272.4 ± 2.91	180.3 ± 1.93	101.9 ± 1.09
154.7 ± 3.18	11.030 ± 0.012	6.145 ± 0.006	6.017 ± 0.007	11.142 ± 0.007	11.119 ± 0.015	42.72 ± 0.20	21.97 ± 0.19	19.00 ± 0.16	20.10 ± 0.21	21.83 ± 0.18	45.04 ± 0.20	42.38 ± 0.20	0.954 ± 0.003	14.20 ± 0.20	15.83 ± 0.20	1.553 ± 0.003	174.1 ± 1.86	243.5 ± 2.60	256.6 ± 2.74	168.3 ± 1.80
123.2 ± 3.16	10.966 ± 0.012	6.142 ± 0.006	6.029 ± 0.007	11.053 ± 0.007	11.045 ± 0.015	42.47 ± 0.20	21.96 ± 0.19	19.00 ± 0.16	20.21 ± 0.21	21.87 ± 0.18	45.04 ± 0.20	42.35 ± 0.20	0.955 ± 0.003	14.16 ± 0.20	15.81 ± 0.20	1.554 ± 0.003	192.0 ± 2.05	259.0 ± 2.77	230.6 ± 2.46	143.4 ± 1.53
63.7 ± 3.13	10.624 ± 0.012	6.271 ± 0.006	6.217 ± 0.007	10.699 ± 0.007	10.701 ± 0.015	41.92 ± 0.20	23.13 ± 0.19	20.46 ± 0.16	22.30 ± 0.21	23.08 ± 0.18	45.07 ± 0.20	42.37 ± 0.20	0.957 ± 0.003	15.68 ± 0.20	17.68 ± 0.20	1.263 ± 0.003	215.3 ± 2.30	280.0 ± 2.99	176.8 ± 1.89	98.4 ± 1.05
79.4 ± 3.14	10.521 ± 0.012	6.198 ± 0.006	6.126 ± 0.007	10.604 ± 0.007	10.592 ± 0.015	41.41 ± 0.20	22.57 ± 0.19	20.05 ± 0.16	21.70 ± 0.21	22.52 ± 0.18	45.11 ± 0.20	41.48 ± 0.20	0.639 ± 0.003	15.72 ± 0.20	17.47 ± 0.20	1.324 ± 0.003	175.1 ± 1.87	244.6 ± 2.61	186.2 ± 1.99	108.3 ± 1.16
158.0 ± 3.19	12.414 ± 0.012	6.334 ± 0.006	6.184 ± 0.007	12.505 ± 0.007	12.488 ± 0.015	47.82 ± 0.20	23.37 ± 0.19	20.58 ± 0.16	21.73 ± 0.21	23.12 ± 0.18	49.92 ± 0.20	47.77 ± 0.20	1.662 ± 0.003	15.63 ± 0.20	17.30 ± 0.20	2.065 ± 0.003	309.9 ± 3.31	357.1 ± 3.82	294.6 ± 3.15	178.2 ± 1.90
89.7 ± 3.14	12.231 ± 0.012	6.311 ± 0.006	6.207 ± 0.007	12.304 ± 0.007	12.273 ± 0.015	48.41 ± 0.20	29.65 ± 0.19	20.53 ± 0.16	21.83 ± 0.21	27.62 ± 0.18	49.93 ± 0.20	47.74 ± 0.20	1.663 ± 0.003	15.64 ± 0.20	17.36 ± 0.20	2.051 ± 0.003	459.1 ± 4.91	462.3 ± 4.94	226.7 ± 2.42	123.6 ± 1.32
139.3 ± 3.17	12.389 ± 0.012	6.333 ± 0.006	6.195 ± 0.007	12.481 ± 0.007	12.453 ± 0.015	47.76 ± 0.20	23.40 ± 0.19	20.59 ± 0.16	21.78 ± 0.21	23.19 ± 0.18	49.93 ± 0.20	47.79 ± 0.20	1.661 ± 0.003	15.64 ± 0.20	17.34 ± 0.20	2.070 ± 0.003	334.8 ± 3.58	376.1 ± 4.02	276.0 ± 2.95	163.2 ± 1.74

120.3 ± 3.16	12.377 ± 0.012	6.343 ± 0.006	6.215 ± 0.007	12.457 ± 0.007	12.435 ± 0.015	47.80 ± 0.20	23.53 ± 0.19	20.69 ± 0.16	21.92 ± 0.21	23.32 ± 0.18	50.01 ± 0.20	47.81 ± 0.20	1.662 ± 0.003	15.63 ± 0.20	17.36 ± 0.20	2.069 ± 0.003	365.1 ± 3.90	397.9 ± 4.25	258.4 ± 2.76	148.2 ± 1.58
101.8 ± 3.15	12.310 ± 0.012	6.351 ± 0.006	6.234 ± 0.007	12.363 ± 0.007	12.360 ± 0.015	47.73 ± 0.20	24.04 ± 0.19	20.76 ± 0.16	22.04 ± 0.21	23.83 ± 0.18	50.05 ± 0.20	47.76 ± 0.20	1.662 ± 0.003	15.63 ± 0.20	17.41 ± 0.20	2.065 ± 0.003	402.8 ± 4.30	424.2 ± 4.53	239.3 ± 2.56	133.3 ± 1.42
175.5 ± 3.15	12.498 ± 0.012	6.363 ± 0.006	6.208 ± 0.007	12.635 ± 0.007	12.592 ± 0.015	48.08 ± 0.20	23.49 ± 0.19	20.74 ± 0.16	22.04 ± 0.21	23.22 ± 0.18	50.09 ± 0.20	47.96 ± 0.20	1.662 ± 0.003	15.67 ± 0.20	17.42 ± 0.20	1.982 ± 0.003	292.7 ± 3.13	343.8 ± 3.67	316.9 ± 3.39	195.9 ± 2.09
126.8 ± 3.20	15.126 ± 0.012	7.118 ± 0.006	6.953 ± 0.007	15.202 ± 0.007	15.180 ± 0.015	56.07 ± 0.20	28.12 ± 0.19	23.77 ± 0.16	25.38 ± 0.21	27.82 ± 0.18	59.45 ± 0.20	56.13 ± 0.20	1.570 ± 0.003	16.86 ± 0.20	19.42 ± 0.20	1.929 ± 0.003	577.5 ± 6.17	488.4 ± 5.22	333.3 ± 3.56	163.1 ± 1.74
199.8 ± 3.16	15.594 ± 0.012	7.168 ± 0.006	6.953 ± 0.007	15.729 ± 0.007	15.690 ± 0.015	57.04 ± 0.20	27.54 ± 0.19	23.89 ± 0.16	25.40 ± 0.21	27.17 ± 0.18	60.08 ± 0.20	56.79 ± 0.20	1.571 ± 0.003	16.86 ± 0.20	19.49 ± 0.20	1.928 ± 0.003	461.0 ± 4.93	421.7 ± 4.51	435.4 ± 4.65	223.2 ± 2.38
151.1 ± 3.23	15.437 ± 0.012	7.160 ± 0.006	6.974 ± 0.007	15.565 ± 0.007	15.509 ± 0.015	56.70 ± 0.20	27.63 ± 0.19	23.94 ± 0.16	25.45 ± 0.21	27.34 ± 0.18	60.08 ± 0.20	56.73 ± 0.20	1.566 ± 0.003	16.86 ± 0.20	19.48 ± 0.20	1.929 ± 0.003	531.4 ± 5.68	463.4 ± 4.95	369.1 ± 3.94	183.3 ± 1.96
243.7 ± 3.18	15.743 ± 0.012	7.181 ± 0.006	6.934 ± 0.007	15.872 ± 0.007	15.850 ± 0.015	57.41 ± 0.20	27.58 ± 0.19	23.94 ± 0.16	25.30 ± 0.21	27.13 ± 0.18	60.11 ± 0.20	56.92 ± 0.20	1.574 ± 0.003	16.84 ± 0.20	19.34 ± 0.20	1.929 ± 0.003	402.9 ± 4.30	386.5 ± 4.13	476.2 ± 5.09	258.3 ± 2.76
175.8 ± 3.28	15.575 ± 0.012	7.162 ± 0.006	6.961 ± 0.007	15.640 ± 0.007	15.618 ± 0.015	56.94 ± 0.20	27.54 ± 0.19	23.89 ± 0.16	25.37 ± 0.21	27.19 ± 0.18	60.18 ± 0.20	56.83 ± 0.20	1.565 ± 0.003	16.82 ± 0.20	19.44 ± 0.20	1.930 ± 0.003	491.9 ± 5.26	439.9 ± 4.70	403.5 ± 4.31	203.4 ± 2.17
193.0 ± 3.20	18.019 ± 0.012	7.646 ± 0.006	7.384 ± 0.007	18.141 ± 0.007	18.120 ± 0.015	63.23 ± 0.20	29.93 ± 0.19	26.03 ± 0.16	27.73 ± 0.21	29.51 ± 0.18	67.83 ± 0.20	62.83 ± 0.20	1.515 ± 0.003	16.87 ± 0.20	21.18 ± 0.20	1.818 ± 0.003	723.2 ± 7.73	574.5 ± 6.14	530.5 ± 5.67	228.3 ± 2.44
173.9 ± 3.21	17.957 ± 0.012	7.499 ± 0.006	7.228 ± 0.007	18.055 ± 0.007	18.061 ± 0.015	63.14 ± 0.20	29.61 ± 0.19	25.12 ± 0.16	26.95 ± 0.21	29.14 ± 0.18	68.10 ± 0.20	63.47 ± 0.20	1.518 ± 0.003	17.00 ± 0.20	20.10 ± 0.20	2.175 ± 0.003	802.5 ± 8.57	617.9 ± 6.60	504.6 ± 5.39	213.3 ± 2.28
209.7 ± 3.20	18.328 ± 0.012	7.774 ± 0.006	7.499 ± 0.007	18.394 ± 0.007	18.383 ± 0.015	63.88 ± 0.20	30.46 ± 0.19	26.62 ± 0.16	28.26 ± 0.21	30.01 ± 0.18	68.40 ± 0.20	63.53 ± 0.20	1.515 ± 0.003	17.32 ± 0.20	21.49 ± 0.20	1.662 ± 0.003	701.0 ± 7.49	561.6 ± 6.00	558.4 ± 5.97	243.3 ± 2.60
239.7 ± 3.24	21.486 ± 0.012	8.077 ± 0.006	7.657 ± 0.007	21.628 ± 0.007	21.606 ± 0.015	71.02 ± 0.20	32.01 ± 0.19	27.17 ± 0.16	29.28 ± 0.21	31.35 ± 0.18	74.81 ± 0.20	71.19 ± 0.20	2.538 ± 0.003	17.13 ± 0.20	21.20 ± 0.20	2.088 ± 0.003	1036.1 ± 11.07	732.3 ± 7.82	770.5 ± 8.23	288.3 ± 3.08
243.6 ± 3.28	21.069 ± 0.012	8.012 ± 0.006	7.605 ± 0.007	21.175 ± 0.007	21.186 ± 0.015	70.16 ± 0.20	31.61 ± 0.19	27.05 ± 0.16	29.02 ± 0.21	30.99 ± 0.18	74.97 ± 0.20	69.15 ± 0.20	1.527 ± 0.003	17.12 ± 0.20	21.08 ± 0.20	2.076 ± 0.003	963.7 ± 10.30	697.1 ± 7.45	744.6 ± 7.96	288.4 ± 3.08
199.3 ± 3.28	20.633 ± 0.012	7.819 ± 0.006	7.458 ± 0.007	20.749 ± 0.007	20.739 ± 0.015	69.62 ± 0.20	37.06 ± 0.19	25.61 ± 0.16	27.53 ± 0.21	34.02 ± 0.18	74.98 ± 0.20	69.27 ± 0.20	1.525 ± 0.003	17.02 ± 0.20	20.79 ± 0.20	2.085 ± 0.003	1157.9 ± 12-37	790.5 ± 8.45	642.5 ± 6.87	243.3 ± 2.60
213.7 ± 3.23	20.746 ± 0.012	7.908 ± 0.006	7.528 ± 0.007	20.949 ± 0.007	20.933 ± 0.015	69.65 ± 0.20	31.92 ± 0.19	26.38 ± 0.16	28.19 ± 0.21	31.20 ± 0.18	75.01 ± 0.20	69.19 ± 0.20	1.526 ± 0.003	17.03 ± 0.20	20.96 ± 0.20	2.077 ± 0.003	1047.6 ± 11.19	738.4 ± 7.89	674.0 ± 7.20	258.3 ± 2.76
228.0 ± 3.26	20.954 ± 0.012	7.982 ± 0.006	7.591 ± 0.007	21.116 ± 0.007	21.095 ± 0.015	69.95 ± 0.20	31.64 ± 0.19	26.91 ± 0.16	28.87 ± 0.21	31.02 ± 0.18	75.01 ± 0.20	69.20 ± 0.20	1.526 ± 0.003	17.10 ± 0.20	21.03 ± 0.20	2.080 ± 0.003	1005.2 ± 10.74	717.8 ± 7.67	706.6 ± 7.55	273.3 ± 2.92
123.4 ± 3.16	16.176 ± 0.012	7.779 ± 0.006	7.606 ± 0.007	16.21 ± 0.007	16.23 ± 0.015	60.77 ± 0.20	40.23 ± 0.19	25.57 ± 0.16	28.22 ± 0.21	36.16 ± 0.18	63.30 ± 0.20	60.16 ± 0.20	1.735 ± 0.003	14.56 ± 0.20	18.72 ± 0.20	1.166 ± 0.003	699.3 ± 7.47	559.4 ± 5.98	368.4 ± 3.94	176.8 ± 1.89
178.8 ± 3.21	20.147 ± 0.012	8.004 ± 0.006	7.697 ± 0.007	20.29 ± 0.007	20.30 ± 0.015	74.35 ± 0.20	46.36 ± 0.19	27.26 ± 0.16	29.48 ± 0.21	39.97 ± 0.18	75.00 ± 0.20	71.88 ± 0.20	2.500 ± 0.003	16.64 ± 0.20	21.41 ± 0.20	1.518 ± 0.003	1225.2 ± 13.09	832.9 ± 8.90	638.5 ± 6.82	228.4 ± 2.44
67.5 ± 3.13	10.664 ± 0.012	6.228 ± 0.006	6.162 ± 0.007	10.73 ± 0.007	10.71 ± 0.015	44.56 ± 0.20	29.47 ± 0.19	19.70 ± 0.16	21.10 ± 0.21	27.18 ± 0.18	45.05 ± 0.20	43.04 ± 0.20	1.395 ± 0.003	14.42 ± 0.20	16.47 ± 0.20	1.336 ± 0.003	316.9 ± 3.39	409.2 ± 4.37	183.5 ± 1.96	98.4 ± 1.05
48.5 ± 3.12	9.078 ± 0.012	6.084 ± 0.006	6.050 ± 0.007	9.14 ± 0.007	9.12 ± 0.015	39.09 ± 0.20	27.85 ± 0.19	19.45 ± 0.16	21.94 ± 0.21	26.09 ± 0.18	39.84 ± 0.20	37.01 ± 0.20	0.630 ± 0.003	15.69 ± 0.20	17.24 ± 0.20	1.172 ± 0.003	147.7 ± 1.58	250.6 ± 2.68	147.5 ± 1.58	78.6 ± 0.84
84.6 ± 3.14	12.066 ± 0.012	6.278 ± 0.006	6.183 ± 0.007	12.11 ± 0.007	12.11 ± 0.015	49.62 ± 0.20	31.17 ± 0.19	20.37 ± 0.16	21.57 ± 0.21	28.24 ± 0.18	49.94 ± 0.20	47.79 ± 0.20	1.662 ± 0.003	15.62 ± 0.20	17.27 ± 0.20	2.039 ± 0.003	457.8 ± 4.89	460.9 ± 4.92	217.5 ± 2.32	118.5 ± 1.27
134.4 ± 3.17	16.215 ± 0.012	6.716 ± 0.006	6.535 ± 0.007	16.34 ± 0.007	16.32 ± 0.015	67.75 ± 0.20	40.56 ± 0.19	22.15 ± 0.16	23.11 ± 0.21	33.73 ± 0.18	68.15 ± 0.20	64.55 ± 0.20	1.675 ± 0.003	15.65 ± 0.20	18.27 ± 0.20	2.056 ± 0.003	896.7 ± 9.58	659.7 ± 7.05	389.2 ± 4.16	178.2 ± 1.90